Title: The NAD-booster nicotinamide riboside potently stimulates hematopoiesis through increased mitochondrial clearance

Authors:
N. Vannini[1,2]*‡, V. Campos[1]*, M. Girotra[2,3], V. Trachsel[3], S. Rojas-Sutterlin[1], J. Tratwal[1], S. Ragusa[2], E. Stefanidis[2,4], D. Ryu[5]†, P.Y. Rainer[6], G. Nikitin[3], S. Giger[3], Y.L. Terytty[5], A. Semilietof [2,4], A. Oggier[1], Y. Yersin[1], L. Tauzin[7], E. Pirinen[5]†, W.C. Cheng[2], J. Ratajczak[8], C. Canto[8,9], M. Ehrbar[10], F. Sizzano[8], T.V. Petrova[2,11], D.Vanhecke[2], L. Zhang[2]†, P. Romero[2], A. Nahimana[12], S. Cherix[13], M.A. Duchosal[12], P.C. Ho[2], B. Deplancke[6], G.Coukos[2,11], J. Auwerx[5], M. P. Lutolf [3,14] and O. Naveiras[1,11,12]‡

Affiliations:

[1] Laboratory of Regenerative Hematopoiesis, Swiss Institute for Experimental Cancer Research (ISREC) & Institute of Bioengineering (IBI), School of Life Sciences, Ecole Polytechnique Fédérale de Lausanne (EPFL); Lausanne, Switzerland.

[2] Department of Oncology UNIL CHUV, Ludwig Institute for Cancer Research Lausanne, University of Lausanne, Epalinges 1066, Switzerland.

[3] Laboratory of Stem Cell Bioengineering, Institute of Bioengineering, Ecole Polytechnique Fédérale de Lausanne (EPFL); Lausanne, Switzerland.

[4] Department of Molecular Biology and Genetics, Democritus University of Thrace, Alexandroupolis, Greece

[5] Laboratory of Integrative and Systems Physiology, Institute of Bioengineering, Ecole Polytechnique Fédérale de Lausanne (EPFL); Lausanne, Switzerland.

[6]Laboratory of System Biology and Genetics, Institute of Bioengineering, Ecole Polytechnique Fédérale de Lausanne (EPFL); Lausanne, Switzerland.

[7] Flow Cytometry Platform, School of Life Sciences, Ecole Polytechnique Fédérale de Lausanne (EPFL), Lausanne, Switzerland.

[8] Nestlé Research, EPFL Innovation Park, 1015 Lausanne, Switzerland

[9] School of Life Sciences, Ecole Polytechnique Fédérale de Lausanne (EPFL); Lausanne, Switzerland.

[10] Department of Obstetrics, University Hospital Zürich, University of Zürich, Zürich, Switzerland.

[11] Swiss Institute for Experimental Cancer Research (ISREC), School of Life Sciences. Swiss Federal Institute of Technology Lausanne (EPFL), Lausanne, Switzerland.

[12] Service and Central Laboratory of Hematology, Departments of Oncology and of Laboratories, Centre Hospitalier Universitaire Vaudois (CHUV), Lausanne, Switzerland.

[13] Service d'orthopédie et de traumatologie, Centre Hospitalier Universitaire Vaudois (CHUV), Lausanne, Switzerland

[14] Institute of Chemical Sciences and Engineering, School of Basic Sciences, Ecole Polytechnique Fédérale de Lausanne (EPFL); Lausanne, Switzerland.

† Current addresses: D.R.: Department of Molecular Cell Biology, Sungkyunkwan University School of Medicine, Suwon 16419, Republic of Korea. E.P.: Molecular Neurology, Research Programs Unit, University of Helsinki; Helsinki, Finland. W.C.C.: Healthy Aging Korean MRC, School of Korean Medicine, Pusan National University, 50612, Yangsan, Republic of Korea. L.Z.: Center for Systems Medicine, Institute of Basic Medical Sciences, Chinese Academy of Medical Sciences and Peking Union Medical College, 100005 Beijing, China & Suzhou Institute of Systems Medicine, Suzhou, Jiangsu 215123, China.

‡ Co-corresponding authors olaia.naveiras@epfl.ch (*Lead Contact*) and nicola.vannini@unil.ch.

* These authors contributed equally

Summary:

It has been recently shown that increased oxidative phosphorylation, as reflected by increased mitochondrial activity, together with impairment of the mitochondrial stress response can severely compromise hematopoietic stem cell (HSC) regeneration. Here we show that the NAD^+-boosting agent Nicotinamide Riboside (NR) reduces mitochondrial activity within HSCs through increased mitochondrial clearance, leading to increased asymmetric HSC divisions. NR dietary supplementation results in a significantly enlarged pool of progenitors, without concurrent HSC exhaustion, improves survival by 80%, and accelerates blood recovery after murine lethal irradiation and limiting-HSC transplantation. In immune-deficient mice, NR increased the production of human leucocytes from hCD34+ progenitors. Our work demonstrates for the first time a positive effect of NAD+ boosting strategies on the most primitive blood stem cells, establishing a link between HSC mitochondrial stress, mitophagy and stem cell fate decision, and unveiling the potential of NR to improve recovery of patients suffering from hematological failure including post-chemo/radiotherapy.

Keywords: Hematopoietic stem cell; HSC; long-term hematopoietic stem cell; mitochondria; mitochondrial clearance; mitochondrial recycling; autophagy; Mitophagy; mitonuclear protein imbalance; unfolded protein response mitochondria; UPRmt; asymmetric stem cell division; hematopoietic stem cell transplantation; bone marrow transplantation; bone marrow failure; bone marrow aplasia; human CD34+ progenitors; immune thrombocytopenia; Aplastic Anemia; chemotherapy; radiotherapy; myelodysplasia; myelodysplastic syndrome

INTRODUCTION:

A remarkably small pool of hematopoietic stem cells (HSCs) is responsible for the production of a staggering 10^{11} mature blood cells per day (Catlin et al., 2011; Busch et al., 2015). HSCs are predominantly quiescent during homeostasis (Wilson et al., 2008), entering the cell cycle in response to the physiological demands of the blood-producing system. Consistent with their quiescent state, most HSCs exhibit a relatively low mitochondrial potential and low NAD^+/NADH content, reflecting their glycolysis-driven metabolic profile when residing in their homeostatic hypoxic niche (Simsek et al., 2010; Takubo et al., 2013; Yu et al., 2013). Stress-induced hematopoiesis occurs after extensive injury of intermediate progenitors and their terminally differentiated progeny: platelets, red blood cells and/or leucocytes, which induces rapid proliferation of HSCs to replenish the depleted progenitor populations. HSC transplantation, a procedure where HSCs from an immune-compatible donor are transferred intravenously to a host that has received a lethal dose of radiation or chemotherapy, constitutes the best-characterized model of stress-induced hematopoiesis (reviewed in Purton and Scadden, 2007). One single long-term (LT) HSC can actually reconstitute the whole hematopoietic system of a mouse in these conditions (Osawa et al., 1996). In humans, HSC transplantation has become the first and most extensively exploited stem cell therapy to date, and the only curative regime for most types of leukemia and aggressive lymphomas (Gratwohl, Baldomero and Passweg, 2013). However, the slow nature of hematopoietic recovery still translates into up to 25% toxicity-associated mortality, in large part due to the severe infections that accompany the period of bone marrow (BM) and immune aplasia (Gratwohl et al., 2009; Gooley et al., 2010).

The proliferative stress imposed on HSCs to reconstitute the full hematopoietic system in the 3-6 weeks following HSC transplantation entails activation of oxidative phosphorylation within

mitochondria (Suda et al. 2011), interferes with pyruvate dehydrogenase kinase (PDK) and hypoxia-inducible factor (HIFα)-driven metabolic checkpoints of HSC self-renewal (Takubo et al., 2013; Yu et al. 2013) and thus induces premature HSC aging (Ito et al., 2004). In turn, activation of the mitochondrial stress response, and more specifically of the mitochondrial unfolded protein response (UPR^{mt}), has been shown to enhance mitochondrial health and to prolong lifespan from *C. elegans* to mice (Houtkooper et al., 2013). In conditions where mitochondrial activity is boosted, a two-step stress signaling pathway is initiated, involving an early UPR^{mt} induction and a delayed ROS-mediated Foxo/DAF-16 activation that can promote lifespan extension in *C. elegans* (Mouchiroud et al., 2013). Indeed, FOXO3-mediated autophagy initiation together with activation of the mitochondrial stress response has been shown to act as a metabolic checkpoint that regulates HSCs maintenance (Mohrin et al. 2015; Warr et al. 2013; Hu et al. 2018).

We set out to test whether a clinically-compatible pharmacological strategy to induce the mitochondrial stress response would improve HSC mitochondrial homeostasis and improve hematological reconstitution after HSC transplantation. We chose a NAD^+-boosting strategy because it has been characterized as a means of activating the SIRT1 axis via the induction of the mitochondrial stress response in the context of aging, liver and muscle regeneration (Imai et al., 2000); Belenky et al. 2007; Cantó et al., 2012; Mouchiroud et al., 2013; Zhang et al., 2016). Interestingly, the NAD^+ precursor Nicotinamide (NAM) has been shown to increase the homing of hematopoietic progenitors and to enhance platelet formation *in vitro* (Giammona et al., 2009; Peled et al. 2012; Horwitz et al. 2014), but efforts to use NAM supplementation to enhance hematopoiesis *in vivo* have failed (Konieczna et al., 2013). Here we reveal the ability of a different NAD+ boosting agent, nicotinamide riboside (NR), to reduce mitochondrial potential in

HSCs and enhance hematopoiesis *in vivo* via activation of autophagy, increased mitochondrial clearance and increased proliferative asymmetry in LT-HSCs through the NR-*Nrk*1/2-NMN axis.

RESULTS AND DISCUSSION

Mice supplemented with Nicotinamide Riboside expand the hematopoietic progenitor compartments

Nicotinamide Riboside (NR) was recently identified as a *bona-fide* NAD^+ vitamin B_3 precursor in vertebrates, naturally present in milk and indirectly quantifiable in plasma (Trammell et al., 2016 and Bogan and Brenner 2008). NR uses a dedicated transporter and enters the NAD^+ salvage pathway via the NR kinase (Nrk1/2)-mediated phosphorylation of NR into nicotinamide mononucleotide, NMN (reviewed in Bogan and Brenner, 2008, and Cantó et al. 2015). Transcripts associated with the enzymatic machinery necessary to directly incorporate NR onto the NAD salvage pathway, most notably *Nmnat3* and *Nrk1,* are expressed in both long-term (LT) and short-term (ST-) HSCs in homeostatic conditions (Figure S1A; Seita et al., 2012). We provided dietary NR supplementation to mice for seven days (Figure 1A), and found increased BM cellularity (Figure S1B) accompanied by expansion of all short-term hematopoietic progenitors (ST-HSCs, MPPs, CMPs and MEPs, see Figure 1B). Short-term reconstitution 4 weeks after competitive BM transplantation (Figure 1C) and *in vitro* colony forming unit (CFU) assays (Figure 1D) confirmed a functional increase of short-term hematopoietic progenitors upon NR treatment. Importantly, NR did not significantly affect the most primitive, self-renewing compartment of LT-HSCs, whose overall number and function did not change as measured phenotypically by surface marker and functionally by competitive repopulation 16 weeks after BM transplantation (Figure 1B and Figure S1C). Analysis of terminally differentiated blood cells

in NR-treated mice showed a significant increase in circulating platelets, monocytes and granulocytes, although still within the physiological range for C57BL/6 mice (Figure 1E, Figure S1D). Niagen, a food supplement containing GMP-grade NR chloride for human use, induced the same effect on baseline blood counts, although more moderately than our custom-synthetized NR triflate (2.4g of NR per Kg of food) (Figure 1E and Figure S1D). Interestingly, mice receiving food supplemented with NAD precursors with independent entry points within the NAD+ salvage pathway, such as nicotinic acid (NA) and nicotinamide (NAM), did not display any significant differences in their hematopoietic compartments after the same seven-day treatment, indicating that the effect on the hematopoietic system is specific to NR and not to other NAD precursors (Figure S2A-H). Conversely, mice supplemented with NMN, which constitutes the first intracellular intermediate of NR metabolism upon NRK-mediated phosphorylation of NR, exhibited a significant expansion of the hematopoietic progenitor compartments (Figure S3A-C). Hematopoietic progenitor pools were not affected by NR supplementation in *Nrk1-/-;Nrk2-/-* double knockout mice (Figure S3D-F; Fletcher et al. 2017), indicating a specific role of the NR-*Nrk*1/2-NMN axis on NAD-driven hematopoietic progenitor expansion.

We conclude from this data that NR and NMN dietary supplementation expands the ST-HSC and committed hematopoietic progenitors within the murine BM, without significantly affecting the size of the LT-HSC pool.

NR decreases mitochondrial membrane potential (ΔΨm) independently of cell cycle quiescence

Because NR has been shown to enhance mitochondrial fitness (Cantó et al., 2012), we tested its capacity to modify mitochondrial homeostasis. We expected NR to increase mitochondrial activity and biogenesis in HSCs, as it does in mammalian hepatocytes and skeletal muscle through the activation of Sirt1 and its downstream target, PGC1α (Cantó et al., 2015). We isolated HSCs from one-week NR-treated mice and stained them with the mitochondrial membrane potential (ΔΨm) sensitive dye tetramethylrhodamine methyl ester (TMRM). Unexpectedly, we found a striking decrease in ΔΨm both in LT- and ST-HSCs after *in vivo* treatment (Figure 2A). Of note, the expression of *Sirt1* remained unchanged (Figure 2B). To test whether the unexpected NR-mediated decrease in ΔΨm was cell-autonomous, we exposed dividing HSCs to NR *in vitro* for 2 days and again detected a decrease in ΔΨm as compared to controls, which persisted when separately analyzing LT- and ST-HSCs (Figure 2C and S4A,B). The NR-mediated decrease in ΔΨm was dose-dependent and also occurred in HSCs exposed to NMN, the first intracellular intermediate of NR metabolism (Figure S4B). We thus concluded that the NR-mediated decrease in ΔΨm is cell-autonomous in HSCs. Blocking the ABC transporters expressed in HSCs*, Brcp1* and *Mdr 1a/b*, through verapamil treatment only mildly affected NR-induced ΔΨm decrease (Figure S4C), thus indicating that ABC-transporter-mediated dye efflux in HSCs does not explain the NR-induced reduction in TMRM stainings (Goodell et al., 1996; de Almeida et al., 2017). In order to investigate if the mitochondrial phenotype was associated to cell cycle arrest, we exposed both LT-HSCs and ST-HSCs to NR *in vitro* and used a cell-labelling strategy based on carboxy-fluoresceinsuccinimidyl ester (CFSE) to measure ΔΨm in cells that had divided one time (Vannini et al., 2016). NR-exposure slowed

entry into first division for both LT-HSCs and ST-HSCs, but the majority of cells divided after 2 days of culture (Figure 2D). Within the cells that underwent first division, the proportion of LT-HSCs and ST-HSCs that exhibited a low ΔΨm (termed here $TMRM^{low}$) was significantly increased by exposure to NR (Figure 2E), whereas non-dividing LT-HSCs did not present changes in ΔΨm, indicating that the NR-mediated decrease in ΔΨm preferentially occurs in dividing HSCs. Of note, we have previously demonstrated that the $TMRM^{low}$ HSC subset contains, after first division in the same conditions, the functional self-renewing HSC subset (Vannini et al., 2016). We thus conclude that NAD^+ boosting via NR reduces ΔΨm in LT and ST-HSCs in a cell-autonomous manner, independently of cell-cycle quiescence, and preferentially in dividing cells.

NR decreases ΔΨm in human CD34+ cells and improves human blood reconstitution.

As NR was found capable of strongly modulating mitochondrial homeostasis, a key player of HSCs function (Ito et al. 2016, Vannini et al. 2016, Jin et al. 2018), we decided to evaluate the effect of NR on human CD34+ hematopoietic progenitor cells. Since a decrease in ΔΨm is associated with improved HSC function both in mouse and in human (Mantel et al. 2010, Simsek et al. 2010, Vannini et al. 2016), we first tested the effect of NR on murine HSCs in primary and secondary CFUs and demonstrated the ability of NR to improve CFU re-plating efficiency (Figure S4D) without affecting cell viability (Figure S4E). We then tested NR treatment on cultured human CD34+ cells. NR decreased ΔΨm of fetal liver, cord blood and adult BM derived human CD34+ (Figure 3A and Figure S4F). Fetal liver derived human CD34+ cells cultured in the presence or absence of NR and transplanted into irradiated NSG recipient mice

engrafted significantly better than controls, and they were capable of sustaining long-term blood production in both primary and secondary recipient NSG mice (Figures 3B and S5). Importantly, analysis of peripheral blood and spleen demonstrated that both the lymphoid and myeloid lineages reconstituted significantly better in mice transplanted with NR-treated CD34+ cells (Figure S5), confirming the superior functionality of NR-treated CD34+ cells and excluding possible lineage biases introduced by NR treatment. BM analysis of primary and secondary recipient NSG mice congruently revealed a higher proportion of human hematopoietic progenitor cells (CD34+ and CD34+CD38-) in the NR treated group than in the control marrow (Figure S5).

Taken together, our data demonstrates that human CD34+ hematopoietic progenitors also exhibit a very significant reduction on ΔΨm upon NR exposure, which improves hematopoietic stem cell function.

NR increases mitochondrial clearance and reduces mitochondrial metabolism.

We then set to investigate the molecular mechanisms underlying the striking mitochondrial phenotype induced by NR treatment in HSCs. RNAseq analysis of *in vitro* cultured LT and ST-HSCs revealed induction of autophagy genes in both cell populations upon NR supplementation (Figure 4A). Increased expression of autophagy-related genes was associated with up-regulation of NAD salvage pathway and *de novo* synthesis genes (Figure 4B) and key mitophagy players, including *Pink1* and *Ulk1*(Figure 4C), (Lazarou et al. 2015). To study whether increased autophagy/mitophagy underlies the NR-mediated decrease in ΔΨm, we treated LT- and ST-HSCs with bafilomycin A1, which inhibits autophagy and mitophagy by blocking the fusion of

autophagosomes and lysosomes. We then quantified the size of Lc3b+ punctae by immunofluorescence to estimate autophagic flux (Mizushima et al., 2010; Warr et al., 2013). Bafilomycin successfully blocked the autophagic flux of control LT-HSCs, as shown by the accumulation of significantly bigger Lc3b+ punctae in comparison to the control cells (Figure S6A). When LT-HSCs were exposed to NR, bafilomycin A1 treatment resulted in restored mitochondrial activity as measured by Mitotracker Deep Red signal in confocal microscopy (Figure 5A) and TMRM staining by FACS (Figure S6B), and a tendency to increased autophagy flux (Figure 5A, and Figure S6A top panel). Note that the accumulation of bigger LC3b+ punctae is more pronounced in LT-HSCs than ST-HSCs upon bafilomycin A1 treatment (Figure S6A bottom panel), indicating a higher basal autophagic flux in the more primitive LT-HSCs as compared to ST-HSCs, consistent with previous data comparing autophagy in HSCs to more committed bipotent granulocyte-monocyte GMP progenitors (Warr et al., 2013; Mortensen et al., 2011). Transplantation of HSCs cultured *in vitro* with Bafilomycin A1 for 48 hours into lethally irradiated mice hampered the NR-mediated HSC gain of function, reestablishing a similar engraftment capacity to untreated cells (Figure S6B). We thus concluded that NR exposure mediates increased mitochondrial clearance in HSCs, an effect which is more pronounced in LT-HSCs.

The NR-mediated increase in HSC mitochondrial clearance was also associated with a significant reduction of all RNA transcripts related to the major mitochondrial energy pathways, including the tricarboxylic acid (TCA) cycle and Oxidative phosphorylation (OxPh) (Figure 5B), while fatty acid oxidation was slightly decreased and glycolysis remained unchanged (Figure 5C). This observation supports the hypothesis that NR-mediated $\Delta\Psi m$ reduction in HSCs is a cooperative process involving mitophagy and metabolic checkpoints, and possibly that these two

processes orchestrate together the clearance of damaged mitochondria to maintain mitochondrial quality control (Park et al. 2015; Ito et al. 2016). Remarkably, in spite of reduced ΔΨm and reduced transcription of the major mitochondrial gene pathways, one of the genes most significantly induced by NR-treatment is the HSC metabolic checkpoint regulator pyruvate dehydrogenase kinase 4 (*PDK4*) (Figure 5D), which catalyzes the inhibitory phosphorylation of pyruvate dehydrogenase (PDH), responsible for the formation of Acetyl-CoA from pyruvate (Harris, Bowker-Kinley et al. 2002). PDK4 has been demonstrated a key metabolic checkpoint for hematopoietic stem cell function and quiescence. Indeed, upregulation of PDK4 reduces the intake of metabolites in the mitochondria, induces mitochondrial clearance via PINK1 stabilization, and thus imposes a more glycolytic cellular metabolism (Takubo et al. 2013, Warr et al. 2013, Park et al. 2015). In order to directly measure changes in the metabolic response of hematopoietic cells in presence of NR, and given the impossibility of sorting a sufficient number of LT-HSCs to perform reproducible seahorse assays, we recurred to analysis of splenocytes as a surrogate assay to measure the effect of NR in oxygen respiration rate (Mantel et al., 2015). Splenocytes exposed to NR displayed a significant reduction in ΔΨm, while exhibiting an increase in respiratory capacity (Figure S6C), indicating that the NR-mediated decrease in ΔΨm is associated to improved metabolic fitness at the cellular level, as previously described in other tissue systems (Palikaras et al., 2015; Ryu et al., 2016).

To determine if NR could actually induce specific mitophagy *in vivo*, we supplemented the diet of mitophagy reporter mice (mito-QC) with NR (McWilliams and Ganley 2016; McWilliams, Prescott et al. 2016). Mito-QC mice express ubiquitously a tandem mCherry-GFP fusion protein fused with mitochondrial outer membrane targeting sequence of FIS1. In steady state mitochondria fluoresce in both red and green. Upon mitophagy induction, however,

mitochondria are delivered to lysosomes where the mCherry signal remains stable, while the GFP signal is quickly quenched by the acidic microenvironment. The GFP-mCherry+ population thus represents a snapshot of cells undergoing active mitophagy (Rizzuto et al. 1995, 1996). Mice whose diet was supplemented with NR presented a higher proportion of LT-HSCs undergoing mitophagy, while no major effect was detected in ST-HSCs (Figure 5E). Downstream hematopoietic progenitors, MPPs (KLS CD150-) and CPs (Lin- cKit+), exhibited lower mitophagy as compared to the most primitive hematopoietic compartments and were unaffected by NR supplementation (Figure S6D). Importantly, the use of this "dye free" system to analyze mitophagy confirms previous studies where mitophagy has been proposed as an important mechanism for HSCs maintenance (Ito et al. 2016, Vannini et al. 2016, Jin et al. 2018, Yang and Suda 2018).

NR induces mitochondrial stress *in vivo*.

We then tested if our NAD+ boosting strategy could induce mitochondrial stress in HSCs, for the mitochondrial stress response has been proposed in other tissues as a regulator of energy homeostasis and increased mitochondrial clearance (Zhang J. et al. 2015; Sorrentino et al., 2017). Similarly to the NR-induced increase in mitochondrial clearance, mRNA levels of mitochondrial-stress-associated chaperones, *Hsp60* and *Hspa9,* as well as of the mitochondrial protease *LonP1* were increased in LT-HSCs from mice whose diet was supplemented with NR, while the effect was more moderate in ST-HSCs (Figure S6E). By Western blotting, we could further observe a mitonuclear protein imbalance specifically in LT-HSCs, but not ST-HSCs-isolated from these mice (Figure S6F). The nuclear-DNA-encoded subunit of Oxphos complex V ATP5a was expressed at equivalent levels in LT- and ST-HSCs regardless of NR treatment. However, the mitochondrial-DNA-encoded MTCO1 protein, a component of Complex IV, was

induced by NR-treatment in LT- but not ST-HSCs, indicating a stoichiometric mitonuclear protein imbalance which could be the trigger for the NR-mediated mitochondrial stress response, as previously suggested (Mouchiroud et al., 2013, Jovaisaite and Auwerx 2015, Leveque-El Mouttie, 2015). We further tested activation of the mitochondrial stress response at the protein level in human hematopoietic stem cell-like leukemic cell line K562, as mitonuclear imbalance has been also described in preleukemic conditions (Schildgen et al. 2011). Increasing concentrations of NR up to 2mM did not affect cell survival over 48h of treatment (Figure S7A). However, NR treatment induced mitonuclear imbalance (MTCO1/SDHA ratio) and mitochondrial stress-associated protein HSP60 in a dose dependent manner (Figure S7B). Of note, there was no increase in K562 leukemic colonies upon NR treatment (data not shown).

We conclude that NR treatment causes a mitonuclear protein imbalance in HSCs and induces the mitochondrial stress response in a cell-autonomous manner, preferentially in the most primitive LT-HSC compartment. The fact that NR-supplementation induces mitochondrial clearance in HSCs, as opposed to the increased mitochondrial activity observed in other mammalian tissues upon NR exposure (Mouchiroud et al. 2013, Khan et al. 2014), is surprising, but points to cell-specificity and directionality of the mitochondrial stress response.

NR promotes asymmetric mitochondrial distribution in LT-HSCs upon cell division

Since both NR-induced mitochondrial clearance and NR-induced activation of the mitochondrial stress response occurred preferentially in the most primitive, dividing LT-HSCs, we postulated that the expansion of short-term progenitors observed in NR-treated mice may be a consequence of altered HSC fate decisions. As the size of the LT-HSC pool remained unchanged upon NR-treatment (Figure 1, Figure S1C) we did not expect an increase in HSC self-renewing divisions,

but hypothesized that NR might increase ST-HSCs and their progeny by increasing asymmetric divisions in HSCs. This hypothesis is consistent with the current view that asymmetric cell division regulates stem cell fate and self-renewal (Morrison and Kimble 2006, Ting, et al. 2012), and that mitochondrial metabolism plays an important role in the modulation of asymmetric cell division in HSCs (Ito, Carracedo et al. 2012). In support of this hypothesis, purified ST-HSCs from mice fed with a NR-supplemented diet showed no increase in cell cycle entry (Figure S6G). Single-cell tracking of NR-treated HSCs showed a significant increase in time-asynchronous divisions (Figure 6A), which has been proposed as an epiphenomenon associated to increased asymmetric stem cell divisions (Vannini et al., 2012). We applied state-of-the-art single cell analysis to evaluate NR-induced asymmetry of cell divisions in HSCs. LT-HSCs were purified from mito-EGFP mice, which express EGFP tagged by the importing signal of the mitochondrial cytochrome *c* oxidase subunit VIII (Rizzuto, Brini et al. 1995, Rizzuto, Brini et al. 1996), thus ubiquitously and exclusively expressing EGFP in the mitochondria (Shitara et al. 2001). By combining the use of mito-EGFP mice and mitochondrial DNA quantification, we could confirm that the more primitive hematopoietic compartments have lower mitochondrial content than the populations of MPP and CP committed progenitors (Figure S7C) (Simsek T. et al. 2010, Vannini et al. 2016). Mito-EGFP LT-HSCs were then sorted by FACS and cultured into a microwell system designed to track both cell division by time lapse microscopy and mitochondrial distribution by confocal imaging (Figure 6B-D) (Abe et al. 2011). Both mitochondrial mass (EGFP) and $\Delta\Psi m$ (TMRM) were measured and analyzed in daughter cells (paired-daughter cells, PDCs) at the end of the culture. The TMRM/EGFP ratio was used as readout for normalized mitochondrial activity (Figure 6B,D). LT-HSCs exposed to NR showed significantly higher asymmetric distribution of active mitochondria in daughter cells as compared to the

control group (Figure 6E). Specifically, log10 asymmetric distribution of active mitochondria in daughter cells happened in 20% of LT-HSCs exposed to NR, as opposed to 7.5% of the cells in control LT-HSCs. These results, combined with our previous study demonstrating that only $TMRM^{low}$ but not $TMRM^{high}$ LT-HSCs retain long-term engrafting capacity after first division *in vitro* (Vannini et al. 2016), support the role of NR in increasing LT-HSC asymmetric divisions and highlight the role of mitochondria as determinants of stem cell fate decision. Recent data from us and others actually demonstrated that maintenance of a low mitochondrial potential through activation of autophagy is necessary to maintain HSC self-renewal (Vannini et al., 2016), a process mediated by PPAR-dependent increase in fatty acid oxidation through enhanced Parkin recruitment in mitochondria (Ito et al., 2016).

These results open important questions in regard to recent publications highlighting higher mitochondrial content in HSCs as compared to more committed progenitor populations and arguing on the role of mitophagy in the maintenance of a functional HSCs pool (de Almeida, Luchsinger et al. 2017, Snoeck 2017). Our data and that of others (Figure S7C; Vannini et al. 2016; Yang and Suda 2018; Jin et al. 2018; Baumgartner et al. 2018) indicate that increased mitochondrial recycling and lower mitochondrial content in the most primitive HSCs associate to enhanced stem cell function, and encourage future studies to better understand the link between mitochondrial dynamics and HSC function and fate.

Improved survival and enhanced blood cell production of post-transplanted mice treated with NR

Finally, as survival after transplantation depends on the formation of sufficient ST-HSCs to maintain rapid stress hematopoiesis (Yang et al., 2005), we tested whether NR supplementation

would be sufficient to accelerate blood recovery following HSC transplantation. Indeed, limiting-dose-HSC transplantation proved lethal for all control mice, while 80% of mice receiving the NR-supplemented diet survived (Figure 7A-B). We further transplanted mice with an excess dose of CD45.1 BM cells, such that survival would not be compromised upon repeated bleeding to monitor blood counts. Platelet and neutrophil recovery were significantly faster in NR-treated mice as compared to controls (Figure 7C-D). Time of exit of severe neutropenia is a critical factor for patient outcome, typically determining hospital discharge. Mice treated with NR supplementation corrected granulocyte counts (neutrophiles > 0.5 G/l), on average, one week before controls (Figure 7D). Recovery from severe thrombocytopenia as defined by platelet count > 200 G/l, which is the functional cutoff for severe bleeding in mice (Morowski et al. 2013), occurred on average 10 days earlier in NR-treated mice (Figure 7C). Increased survival and faster blood recovery were not due to a NR-mediated radio-protective effect, as there was no difference in residual CD45.2 cells from recipient mice (Figure S7D). Importantly, there was no HSC exhaustion after extended NR treatment, as secondary transplants from the marrow of these mice showed equivalent CD45.1 long-term engraftment at 16 weeks (Figure S7E). Lethally irradiated mice transplanted with total bone marrow from mitoQC mice and supplemented with NR in the diet during the entire post-transplant period (similar to Figure 7A) presented higher mitophagic rate in their stem and multipotent progenitor compartments during the blood recovery period (Figure 7E). NR supplementation in stress hematopoiesis is thus coupled to induction of mitophagy in the most primitive hematopoietic compartments.

Finally, humanized mice fed with NR-supplemented diet for one week presented enhanced human hematopoiesis as reflected by a significant increase in lymphocyte (Figure 7F) and possibly monocyte production (Figure S7F). Human neutrophil recovery is unfortunately not

measurable in standard humanized NSG mice (Rongvaux et al., 2014). We thus conclude that NR supplementation accelerates both murine and human hematopoiesis, significantly increasing survival in mice upon limiting-HSC transplantation.

Conclusions and perspectives

Collectively, our work links the NAD salvage pathway to mitochondrial clearance in wildtype HSCs, via induction of mitochondrial stress response and increase in asymmetric divisions. The mitochondrial effects of NAD replenishment *in vivo* were observed at the level of the most primitive HSCs, both during homeostatic and stress hematopoiesis, which demonstrates the cell-type specific directionality of the mitochondrial stress response. Moreover, our results reveal NR and NMN as potential boosters of hematopoiesis which could prove useful either *in vitro* for HSC expansion protocols, such as in the context of expansion for adoptive cell transfer or for increased immune cell metabolic fitness upon immune-therapy, or *in vivo* to reduce mortality in the setting of BM aplasia and possibly in the context of myelodysplastic syndromes where an age-dependent mitochondrial defected has been suggested (Pellagatti et al., 2018). Given the efficient enhancement of megakaryopoiesis, NR supplementation could also prove beneficial for the treatment of refractory autoimmune idiopathic thrombocytopenic purpura (ITP) or other auto-immune BM failure syndromes. Of note, the wide-ranging protective effects of NR on mitochondrial activity in non-hematopoietic tissues would be of additional value for HSC-ablative chemotherapy regimens, which often carry significant secondary cardio/neurotoxicity due to mitochondrial impairment (Bogan et al., 2008; Cantó et al. 2015).

Acknowledgements:

We thank Elena Katsyuba (EPFL), Laurent Mouchiroud (EPFL), Nina Dumauthioz (UNIL) and George Q. Daley (Harvard Medical School) for critical reading of the manuscript, the members of the Center for the Study of Living Systems (EPFL) and Francis Derouet (UNIL) for animal care, Evan Williams for help with normalization of RNA expression data, Evangelos Panopoulos and Magdalena Plotczyk for technical support, Elena Goun for independent NR purity analysis, and Bastian Mangeat at the Genetics Expression Core Facility (EPFL) for RNA sequencing support. Andrea Negro helped with statistical analysis. R.J. Chapman provided Niagen. Flow cytometry analysis / cell sorting was performed both atthe EPFL Flow Cytometry Core Facility with the help of Sintia Winkler, Telma Lopes and Miguel Garcia, and at the Nestlè Institute of Health Sciences (NIHS) Flow Cytometry facility with the help of Filippo de Franceschi and Gabriele Dammone. A special thanks to the EPFL Kebab truck crew for the numerous late meals.

O.N. was supported by the Machaon Foundation, the Dr Henri Dubois-Ferrière Dinu Lipatti Leukemia Foundation, the Fondation Pierre Mercier pour la science, and Swiss National Science Foundation (SNF) Professorship grants PP00P3_144857 and PP00P3_176990. The work performed in the laboratory of M.P.L. was supported by a Swiss National Science Foundation Sinergia grant (CRSII3_147684) and an ERC grant (StG_311422). The work in the JA laboratory was supported by the EPFL and grants from Krebsforschung Schweiz /SwissCancerLeague (KFS-3082-02-2013), Systems X (SySX.ch 2013/153) and SNSF (31003A-140780). The work performed in the laboratory of P.C.H. was supported in part by the Swiss Cancer Foundation (KFS-3949-08-2016) and Swiss National Foundation Project grant (31003A_163204).

Author Contributions : N.V., V.C., M.P.L, J.A. and O.N. conceived ideas, designed experiments, analyzed results and wrote the manuscript. N.V, V.C., O.N., D.R., M.G., S.R., W.C.C, P.C.H and T.V.P. performed and interpreted the murine autophagy and mitochondrial clearance experiments, while M.G., S.G., V.C., Y.L.T., A.N. and M.A.D performed and interpreted human autophagy and mitochondrial clearance experiments. J.R and C.C. provided Nrk1-/-;Nrk2-/- double knock-out mice. M.E. recruited patients and provided cord blood units. S.C. contributed to the design of the human ethical protocol, ensured patient recruitment and provided all adult BM samples. V.T., G.N. and M.P.L. performed and interpreted mito-GFP and asymmetry experiments. O.N., V.C, N.V., S.R.S., J.T., A.O. and Y.Y., performed and interpreted FACS, CFU progenitor and murine in vivo transplantation studies. M.G., E.S., A.S., D.V. and G.C. performed, designed and/or analyzed experiments in humanized mice. L.T., F.S. and A.P. contributed to FACS data acquisition and analysis of murine BM and cord blood. P.Y.R. and B.D. analyzed RNAseq data. L. Z. and P.R. performed OCR experiments. E. P. and J.A. conceived ideas, provided key reagents and comprehensively contributed to experimental design. N.V., M.P.L. and O.N. co-initiated the project. All authors edited and reviewed the final manuscript.

Declaration of Interest : Some elements of this work have been submitted as patent application WO2016038011A1 of which N.V, M.P.L., J.A, O.N and M.G. are inventors. T.P. declares a research grant from Hoffman-La Roche. GC has received grants, research support or is coinvestigator in clinical trials by BMS, Celgene, Boehringer Ingelheim, Roche, Iovance and Kite. GC has provided consultations to Roche, Genentech, BMS, AstraZeneca, Sanofi-Aventis, Nextcure and GeneosTx. J.A. is a founder and SAB member of Mitobridge (an Astellas company).

References :

- Abe, T., Kiyonari, H., Shioi, G., Inoue, K., Nakao, K., Aizawa, S., Fujimori, T. (2011). Establishment of conditional reporter mouse lines at ROSA26 locus for live cell imaging. *Genesis* **49**, 579–590.
- Belenky, P., Racette, F.G., Bogan, K.L., McClure, J.M., Smith, J.S., Brenner. C. (2007). Nicotinamide riboside promotes Sir2 silencing and extends lifespan via Nrk and Urh1/Pnp1/Meu1 pathways to NAD+. *Cell* **129**, 473–484.
- Benjamini, Y., and Hochberg, Y. (1995). Controlling the false discovery rate: a practical and powerful approach to multiple testing. *Journal of the Royal Statistical Society Series B (Methodological)* **57**:289-300.
- Bogan, K.L. and Brenner, C (2008). Nicotinic acid, nicotinamide, and nicotinamide riboside: a molecular evaluation of NAD+ precursor vitamins in human nutrition. *Annu. Rev. Nutr*. **28**,115-130.
- Busch, K., Klapproth, K., Barile, M., Flossdorf, M., Holland-Letz, T., Schlenner, S.M., Reth, M., Höfer, T., Rodewald, H.R. (2015). Fundamental properties of unperturbed haematopoiesis from stem cells in vivo. *Nature* **518**, 542-6.
- Cantó, C., Houtkooper, R.H., Pirinen, E., Youn, D.Y., Oosterveer, M.H., Cen, Y., Fernandez-Marcos, P.J., Yamamoto, H., Andreux, P.A., Cettour-Rose, P., et al (2012). The NAD(+) precursor nicotinamide riboside enhances oxidative metabolism and protects against high-fat diet-induced obesity. *Cell Metab* **15**, 838-47.

- Cantó, C., Menzies, K.J. and Auwerx, J. (2015). NAD(+) Metabolism and the Control of Energy Homeostasis: A Balancing Act between Mitochondria and the Nucleus. *Cell Metab.* **22**,31-53.
- Catlin, S. N., Busque, L., Gale, R. E., Guttorp, P. and Abkowitz, J. L. (2011). The replication rate of human hematopoietic stem cells in vivo. *Blood* **117**, 4460–6.
- De Almeida, M. J., Luchsinger, L. L., Corrigan, D. J., Williams, L. J. and Snoeck H. W. (2017). Dye-Independent Methods Reveal Elevated Mitochondrial Mass in Hematopoietic Stem Cells. *Cell Stem Cell* **21**(6): 725-729.
- Giammona, L.M., Panuganti, S., Kemper, J.M., Apostolidis, P.A., Lindsey, S., Papoutsakis, E.T., Miller, W.M. (2009). Mechanistic studies on the effects of nicotinamide on megakaryocytic polyploidization and the roles of NAD+ levels and SIRT inhibition. *Exp Hematol* **37**, 1340-1352.
- Goodell, M.A., Brose, K., Paradis, G., Conner, A.S., and Mulligan, R.C. (1996). Isolation and functional properties of murine hematopoietic stem cells that are replicating in vivo. *J. Exp. Med.* **183**, 1797–1806.
- Gooley, T.A., Chien, J.W., Pergam, S.A., Hingorani, S., Sorror, M.L. et al. (2010) Reduced mortality after allogeneic hematopoietic-cell transplantation. *N. Engl. J. Med* **363**, 2091–101.
- Gratwohl, A., Stern, M., Brand, R. and Apperley, J. (2009). Risk score for outcome after allogeneic hematopoietic stem cell transplantation. *Cancer* **115**, 4715-26.
- Gratwohl, A., Baldomero, H., Passweg, J. (2013). Hematopoietic stem cell transplantation activity in Europe. *Curr Opin Hematol* **20**, 485-93.

- Harris, R. A., M. M. Bowker-Kinley, B. Huang and P. Wu (2002). Regulation of the activity of the pyruvate dehydrogenase complex. *Adv Enzyme Regul* **42**: 249-259.
- Horwitz, M.E., Chao, N.J., Rizzieri, D.A., Long, G.D., Sullivan, K.M., Gasparetto, C., Chute, J.P., Morris, A., McDonald, C., Waters-Pick, B., et al. (2014). Umbilical cord blood expansion with nicotinamide provides long-term multilineage engraftment. *J. Clin. Invest* **124**, 3121–8.
- Houtkooper, R.H., Mouchiroud, L., Ryu, D., Moullan, N., Katsyuba, E., Knott, G., Williams, R.W., Auwerx, J. (2013). Mitonuclear protein imbalance as a conserved longevity mechanism. *Nature* **497**, 451-7.
- Hu, M., Zeng, H., Chen, S., Xu, Y., Wang, S., Tang, Y., Wang, X., Du, C., Shen, M., Chen, F. et al (2018). SRC-3 is involved in maintaining hematopoietic stem cell quiescence by regulation of mitochondrial metabolism in mice. Blood **132**(9):911-923.
- Imai, S., Armstrong, C.M., Kaeberlein, M., and Guarente, L. (2000). Transcriptional silencing and longevity protein Sir2 is an NAD-dependent histone deacetylase. *Nature* **403**, 795–800.
- Ito, K., Hirao, A., Arai, F., Matsuoka, S., Takubo, K., Hamaguchi, I., Nomiyama, K., Hosokawa, K., Sakurada, K., Nakagata, N., et al. Regulation of oxidative stress by ATM is required for self-renewal of haematopoietic stem cells. (2004). *Nature* **431**, 997–1002.
- Ito, K., A. Carracedo, D. Weiss, F. Arai, U. Ala, D. E. Avigan, Z. T. Schafer, R. M. Evans, T. Suda, C. H. Lee and P. P. Pandolfi (2012). A PML-PPAR-delta pathway for fatty acid oxidation regulates hematopoietic stem cell maintenance. *Nat Med*. **18**:1350-8.
- Ito, K., Turcotte, R., Cui, J., Zimmerman, S.E., Pinho, S., Mizoguchi, T., Arai, F., Runnels, J.M., Alt, C., Teruya-Feldstein, J., et al. (2016). Self-renewal of a purified Tie2+

hematopoietic stem cell population relies on mitochondrial clearance. *Science* **354**, 1156-1160.

- Jensen MB, Jasper H. (2014). Mitochondrial proteostasis in the control of aging and longevity. *Cell Metab.* **20**, 214-225.
- Jin, G., C. Xu, X. Zhang, J. Long, A. H. Rezaeian, C. Liu, M. E. Furth, S. Kridel, B. Pasche, X. W. Bian and H. K. Lin (2018). Atad3a suppresses Pink1-dependent mitophagy to maintain homeostasis of hematopoietic progenitor cells. *Nat Immunol.* **19**: 29-40.
- Jovaisaite, V., Auwerx, J. (2015). The mitochondrial unfolded protein response—synchronizing genomes. *Curr Opin Cell Biol*. **33**, 74-81.
- Khan, N.A., Auranen, M., Paetau, I., Pirinen, E., Euro, L., Forsström, S., Pasila, L., Velagapudi, V., Carroll, C.J., Auwerx, J., Suomalainen, A. (2014). Effective treatment of mitochondrial myopathy by nicotinamide riboside, a vitamin B3. *EMBO molecular medicine* **6**, 721–731.
- Kobel, S., Limacher, M., Gobaa, S., Laroche, T., and Lutolf, M.P. (2009). Micropatterning of hydrogels by soft embossing. *Langmuir* **25**, 8774-9.
- Konieczna, I.M., Panuganti, S., DeLuca, T.A., Papoutsakis, E.T., Eklund, E.A., Miller, W.M. (2013). Administration of nicotinamide does not increase platelet levels in mice. *Blood Cells Mol Dis* **50**, 171-6.
- Lazarou, M., D. A. Sliter, L. A. Kane, S. A. Sarraf, C. Wang, J. L. Burman, D. P. Sideris, A. I. Fogel and R. J. Youle (2015). The ubiquitin kinase PINK1 recruits autophagy receptors to induce mitophagy. Nature **524**, 309-314.

- Leveque-El Mouttie, L., Vu, T., Lineburg, KE., Kuns, R.D., Bagger, F.O., Teal, B.E., Lor, M., Boyle, G.M., Bruedigam, C., Mintern, J.D., et al. (2015). Autophagy is required for stem cell mobilization by G-CSF. *Blood* **125,** 2933–6.
- McWilliams, T. G. and I. G. Ganley (2016). Life in lights: Tracking mitochondrial delivery to lysosomes in vivo. *Autophagy* **12**, 2506-2507.
- McWilliams, T. G., A. R. Prescott, G. F. Allen, J. Tamjar, M. J. Munson, C. Thomson, M. M. Muqit and I. G. Ganley (2016). Mito-QC illuminates mitophagy and mitochondrial architecture in vivo. *J Cell Biol* **214**: 333-345.
- Mantel, C., S. Messina-Graham and H. E. Broxmeyer (2010). Upregulation of nascent mitochondrial biogenesis in mouse hematopoietic stem cells parallels upregulation of CD34 and loss of pluripotency: A potential strategy for reducing oxidative risk in stem cells. *Cell Cycle* **9**, 2008-2017.
- Mantel, C.R., O'Leary, H.A., Chitteti, B.R., Huang, X., Cooper, S., Hangoc, G., Brustovetsky, N., Srour, E.F., Lee, M.R., Messina-Graham, S., et al. (2015). Enhancing Hematopoietic Stem Cell Transplantation Efficacy by Mitigating Oxygen Shock. *Cell* **161**, 1553–1565.
- Mizushima, N, Yoshimori, T, and Levine, B (2010). Methods in mammalian autophagy research. *Cell* **140**, 313-26.
- Mohrin, M., Shin, J., Liu, Y., Brown, K., Luo, H., Xi, Y., Haynes, C.M., Chen, D. (2015). Stem cell aging. A mitochondrial UPR-mediated metabolic checkpoint regulates hematopoietic stem cell aging. *Science* **347**, 1374-7.

- Morowski, M., Vögtle, T., Kraft, P., Kleinschnitz, C., Stoll, G., Nieswandt, B. (2013). Only severe thrombocytopenia results in bleeding and defective thrombus formation in mice. *Blood* **121**, 4938–47.
- Morrison, S. J. and Kimble J. (2006). Asymmetric and symmetric stem-cell divisions in development and cancer. *Nature* **441**(7097): 1068-1074.
- Mortensen, M., Soilleux, E.J., Djordjevic, G., Tripp, R., Lutteropp, M., Sadighi-Akha, E., Stranks, A.J., Glanville, J., Knight S., Jacobsen, S.E. et al. (2011). The autophagy protein Atg7 is essential for hematopoietic stem cell maintenance. *J Exp Med* **208**(3):455-67.
- Mouchiroud, L., Houtkooper, R.H., Moullan, N., Katsyuba, E., Ryu, D., Cantó, C., Mottis, A., Jo, Y.S., Viswanathan, M., Schoonjans, K. et al. (2013). The NAD(+)/Sirtuin Pathway Modulates Longevity through Activation of Mitochondrial UPR and FOXO Signaling. *Cell* **154**, 430-41.
- Osawa, M., Hanada, K.I., Hamada, H., and Nakauchi, H. (1996). Long-term lymphohematopoietic reconstitution by a single CD34-low/negative hematopoietic stem cell. *Science* **273**, 242–245.
- Palikaras, K., Lionaki, E., and Tavernarakis, N. (2015). Coordination of mitophagy and mitochondrial biogenesis during ageing in C. elegans. *Nature* **521**, 525–528.
- Park, S., S. G. Choi, S. M. Yoo, J. Nah, E. Jeong, H. Kim and Y. K. Jung (2015). Pyruvate stimulates mitophagy via PINK1 stabilization. *Cell Signal* **27**(9): 1824-1830.
- Peled, T., Shoham, H., Aschengrau, D., Yackoubov, D., Frei, G., Rosenheimer, G.N., Lerrer, B., Cohen, H.Y., Nagler, A., Fibach, E., Peled, A. (2012). Nicotinamide, a SIRT1 inhibitor, inhibits differentiation and facilitates expansion of hematopoietic progenitor cells with enhanced bone marrow homing and engraftment. *Exp Hematol* **40**, 342–355.

- Pellagatti, A., Armstrong, R.N., Steeples, V., Sharma, E., Repapi, E., Singh, S., Sanchi, A., Radujkovic, A., Horn, P., Dolatshad, H., et al. (2018). Impact of spliceosome mutations on RNA splicing in myelodysplasia: dysregulated genes/pathways and clinical associations. *Blood* ***132***, 1225–1240.
- Purton, L.E., and Scadden, D.T. (2007). Limiting factors in murine hematopoietic stem cell assays. *Cell Stem Cell* **1**, 263–270.
- Fletcher, R.S., Ratajczak, J., Doig, C.L., Oakey, L.A., Callingham, R., Da Silva Xavier, G., Garten, A., Elhassan, Y.S., Redpath, P., Migaud, M.E., et al. (2017). Nicotinamide riboside kinases display redundancy in mediating nicotinamide mononucleotide and nicotinamide riboside metabolism in skeletal muscle cells. *Mol Metab* **6**(8):819-832.
- Rizzuto, R., M. Brini, F. De Giorgi, R. Rossi, R. Heim, R. Y. Tsien and T. Pozzan (1996). Double labelling of subcellular structures with organelle-targeted GFP mutants in vivo. *Curr Biol* **6**: 183-188.
- Rizzuto, R., M. Brini, P. Pizzo, M. Murgia and T. Pozzan (1995). Chimeric green fluorescent protein as a tool for visualizing subcellular organelles in living cells. *Curr Biol* **5**: 635-642.
- Rongvaux, A., Willinger, T., Martinek, J., Strowig, T., Gearty, S.V., Teichmann, L.L., Saito, Y., Marches, F., Halene, S., Palucka, A.K., et al. (2014). Development and function of human innate immune cells in a humanized mouse model. *Nature Biotechnology* **32**, 364-372.
- Ryu, D., Mouchiroud, L., Andreux, P.A., Katsyuba, E., Moullan, N., Nicolet-Dit-Félix, A.A., Williams, E.G., Jha, P., Lo Sasso, G., Huzard, D., et al. (2016). Urolithin A induces

mitophagy and prolongs lifespan in C. elegans and increases muscle function in rodents. *Nat. Med.* **22**, 879–888.

- Schildgen, V., M. Wulfert and N. Gattermann (2011). Impaired mitochondrial gene transcription in myelodysplastic syndromes and acute myeloid leukemia with myelodysplasia-related changes. *Exp Hematol* **39**(6):666-675.
- Seita, J., Sahoo, D., Rossi, D.J., Bhattacharya, D., Serwold, T., Inlay, M.A., Ehrlich, L.I., Fathman, J.W., D.L. Dill and I.L. Weissman. (2012). Gene Expression Commons: an open platform for absolute gene expression profiling. *PLoS ONE* **7**, e40321.
- Shitara, H., H. Kaneda, A. Sato, K. Iwasaki, J. Hayashi, C. Taya and H. Yonekawa (2001). Non-invasive visualization of sperm mitochondria behavior in transgenic mice with introduced green fluorescent protein (GFP). *FEBS Lett* **500**: 7-11.
- Simsek, T., Kocabas, F., Zheng, J., Deberardinis, R.J., Mahmoud, A.I., Olson, E.N., Schneider, J.W., Zhang, C.C., Sadek, H.A. (2010). The distinct metabolic profile of hematopoietic stem cells reflects their location in a hypoxic niche. *Cell Stem Cell* **7**, 380–90.
- Snoeck, H. W. (2017). Mitochondrial regulation of hematopoietic stem cells. *Curr Opin Cell Biol* **49**: 91-98.
- Sorrentino, V., Romani, M., Mouchiroud, L., Beck, J.S., Zhang, H., D'Amico, D., Moullan, N., Potenza, F., Schmid, A.W., Rietsch, S., et al. (2017). Enhancing mitochondrial proteostasis reduces amyloid-β proteotoxicity. *Nature* **552**, 187–193.
- Suda, T., Takubo, K., Semenza, G.L. (2011). Metabolic regulation of hematopoietic stem cells in the hypoxic niche. *Cell Stem Cell* **9**, 298–310.

- Takubo, K., G. Nagamatsu, C. I. Kobayashi, A. Nakamura-Ishizu, H. Kobayashi, E. Ikeda, N. Goda, Y. Rahimi, R. S. Johnson, T. Soga, A. Hirao, M. Suematsu and T. Suda (2013). Regulation of glycolysis by pdk functions as a metabolic checkpoint for cell cycle quiescence in hematopoietic stem cells. *Cell Stem Cell* **12**: 49-61.
- Ting, S. B., E. Deneault, K. Hope, S. Cellot, J. Chagraoui, N. Mayotte, J. F. Dorn, J. P. Laverdure, M. Harvey, E. D. Hawkins, S. M. Russell, P. S. Maddox, N. N. Iscove and G. Sauvageau (2012). Asymmetric segregation and self-renewal of hematopoietic stem and progenitor cells with endocytic Ap2a2. *Blood* **119**: 2510-2522
- Trammell, S.A., Schmidt, M.S., Weidemann, B.J., Redpath, P., Jaksch, F., Dellinger, R.W., Li, Z., Abel, E.D., Migaud, M.E., and Brenner, C. (2016). Nicotinamide riboside is uniquely and orally bioavailable in mice and humans. *Nat Commun* **7**, 12948.
- Vannini, N., Roch, A., Naveiras, O., Griffa, A., Kobel, S., Lutolf, M.P. (2012). Identification of in vitro HSC fate regulators by differential lipid raft clustering. *Cell Cycle* **11,** 1535–43.
- Vannini, N., Girotra, M., Naveiras, O., Nikitin, G., Campos, V., Giger, S., Roch, A., Auwerx, J., and Lutolf, M.P. (2016). Specification of haematopoietic stem cell fate via modulation of mitochondrial activity. *Nat Commun* **7**, 13125.
- Warr, M.R., Binnewies, M., Flach, J., Reynaud, D., Garg, T., Malhotra, R., Debnath, J., Passegué, E. (2013). FOXO3A directs a protective autophagy program in haematopoietic stem cells. *Nature* **494**, 323-7.
- Wilson, A., Laurenti, E,. Oser, G., van der Wath, R.C., Blanco-Bose, W., Jaworski, M., Offner, S., Dunant, C.F., Eshkind, L., Bockamp, E., et al. (2008). Hematopoietic stem cells

reversibly switch from dormancy to self-renewal during homeostasis and repair. *Cell* **135**, 1118-29.

- Yang, L., Bryder, D., Adolfsson, J., Nygren, J., Månsson, R., Sigvardsson, M., Jacobsen, S.E. (2005). Identification of Lin(−) Sca1(+)kit(+) CD34(+)Flt3-short-term hematopoietic stem cells capable of rapidly reconstituting and rescuing myeloablated transplant recipients. *Blood* **105**, 2717–2723.
- Yang, C. and T. Suda (2018). Hyperactivated mitophagy in hematopoietic stem cells. *Nat Immunol* **19**(1): 2-3.
- Yu, W.M., Liu. X-, Shen. J., Jovanovic, O., Pohl, E.E., Gerson, S.L., Finkel, T., Broxmeyer, H.E., Qu, C.K. (2013). Metabolic Regulation by the Mitochondrial Phosphatase PTPMT1 Is Required for Hematopoietic Stem Cell Differentiation. *Cell Stem Cell* **12**, 62-74.
- Zhang H, Ryu D, Wu Y, Gariani K, Wang X, Luan P, D'Amico D, Ropelle ER, Lutolf MP, Aebersold R, Schoonjans K, Menzies KJ, Auwerx J (2016). NAD^+ repletion improves mitochondrial and stem cell function and enhances life span in mice. *Science* **352**(6292), 1436-43.
- Zhang J, Culp ML, Craver JG, Darley-Usmar V (2018). Mitochondrial function and autophagy: integrating proteotoxic, redox, and metabolic stress in Parkinson's disease. *J Neurochem*. **144**(6):691-709.

FIGURE TITLES AND LEGENDS:

Figure 1. NR treatment expands ST hematopoietic progenitors *in vivo*.

A, Mice were fed for 7 days with control or NR diet (12mg NR /mouse/day). Blood was sampled and mice were sacrificed for BM analysis (FACS and CFUs) and secondary transplants. **B,** Phenotypic analysis of the different BM hematopoietic stem/progenitor compartments from control (ctrl) or NR fed mice by flow cytometry, *n=5*; LT-HSCs are *Lineage-cKit+Sca1+(KLS+)CD48-CD150+CD34-*, short-term(ST)-HSCs are *KLS+CD48-CD150+CD34+*, multipotent progenitors (MPPs) are KLS+CD48+, committed progenitors (CPs) include common myeloid progenitors (CMPs: *Lineage-cKit+Sca1-(KLS-) FcR^{low}CD34+),* granulocyte–macrophage progenitors (GMPs: *KLS-FcR^{low}CD34+*) and megakaryocyte–erythroid progenitors (MEPs: *KLS-FcR-CD34-)*. **C,** BM derived from NR- or control-fed mice was transplanted into lethally irradiated mice and peripheral blood chimerism was measured 4 weeks after transplantation, *n=12.* **D,** 12,500 BM cells from ctrl- or NR-fed mice were plated in Methocult for colony forming unit (CFU) analysis 8 days after plating, *n=5*; GEMM, granulocyte-erythroid-monocyte-megakaryocyte mixed CFU; GM, granulocyte-monocyte CFU; M, monocyte CFU; G, granulocyte CFU; Mk, megakaryocyte CFU; E, erythroid and erythroid blast forming CFUs **E**, Blood cell counts of mice fed with ctrl, Niagen or NR diet as in (a.), *n=5*. *Student's t test *p<0.05, **p<0.01, ***p<0.001.* See also Figures S1-S3.

Figure 2. NR treatment decreases mitochondrial membrane potential (ΔΨm).

A, LT and ST-HSC mitochondrial potential measured by TMRM staining, from BM of control- or NR-diet fed mice, *n=5.* **B,** Gene expression analysis of Sirt1 in LT-HSCs derived from control- or NR-diet fed mice, *n=5*. **C,** HSCs were cultured *in vitro* for 2 days in presence or absence of NR and then stained with JC-1 dye, which reports mitochondrial depolarization by a decrease in the red (total mitochondria) to green (active mitochondria) fluorescence intensity ratio. Confocal imaging of JC1 stained mitochondria from HSCs cultured in presence or absence of NR, n=20. **D,** Proportion of dividing and not dividing LT and ST-HSCs as measured by CFSE staining *n=3* **E,** Mitochondrial potential of dividing and not dividing LT and ST-HSCs as measured by TMRM staining in combination with CFSE staining, *n=3. Student's t test *p<0.05, **p<0.01, ***p<0.001.* See also Figure S4A-E.

Figure 3. NR decreases ΔΨm in human CD34+ and improves human blood cell reconstitution. **A,** Human CD34+ cells from fetal liver, cord blood and adult femoral bone marrow were cultured in the presence or absence of NR for 2 days and the $TMRM^{low}$ population (blue outline) and TMRM MFI were quantified by FACS after TMRM staining. Fold changes in MFI are calculated by normalization over control group values. Each data point represents a different donor (fetal liver *n=4,* cord blood *n= 4* with Fig. S4F*,* adult bone marrow *n=5*). **B,** Human CD34+ cells from fetal liver were cultured for 7 days *in vitro* in the presence or absence of 1mM NR and were transplanted in primary (*n=6*) and secondary (*n=12*) recipient NSG mice. Blood reconstitution was analyzed over time while bone marrow (BM) and spleen analysis were performed at the experimental endpoints. *Student's t test *p<0.05, **p<0.01, ***p<0.001.* See also Figures S4F and S5.

Figure 4**. NR induces the expression of autophagy/mitophagy-related genes and NAD salvage pathway. A,** Heatmap of the top 40 up-regulated autophagy-related genes in NR treated LT and ST-HSCs (top panel) and gene enrichment (GE) analysis quantified via enrichment score (ES, bottom panel) (in blue: low expression genes, in red: high expression genes). **B,** Heatmap of NAD salvage pathway gene expression and GE analysis. **C,** Heat-map of mitophagy–related genes produced with *GSEA software analysis.*

Figure 5. NR induces mitophagy and downregulates mitochondrial energy pathways in HSCs

A, Confocal imaging analysis of active mitochondria in sorted LT-HSCs treated with NR +/- autophagy inhibitor bafilomycin A1 for 2 days, as quantified by Mitotracker Deep Red staining, a mitochondrial potential sensitive dye *n=5*. Note that the decrease in mitochondrial mass of active mitochondria upon NR treatment is corrected in the presence of bafilomycin, thus indicating increased mitochondrial clearance in NR-treated LT-HSCs. **B,C,** RNAseq analysis of key energy pathways. Heat map representation (in blue: low expression genes, in red: high expression genes) and gene enrichment analysis are presented. **D,** Volcano plot of gene transcripts most induced by NR treatment in LT- and ST-HSCs. PDK4 metabolic checkpoint expression is highlighted. **E,** Mito-QC mice were supplemented with Ctrl or NR diet for 1 week. Proportion of cells undergoing mitophagy were quantified by flow cytometry measuring mCherry and GFP signal in both LT and ST-HSCs (see text for details) *n=3. Student's t test *p<0.05, **p<0.01, ***p<0.001.* See also Figure S6.

Figure 6. NR induces asymmetric mitochondrial distribution in LT-HSCs. A, Synchrony of cell division analysis in LT-HSCs upon first division was performed by following cell cycle kinetics in the micro-well array system. Cell division was considered asynchronous, thus suggestive of asymmetric HSC divisions, when 2 daughter cells where dividing in a time gap (Δt) > 6h, *n=3.* **B,** LT-HSC paired-daughter cell (PDC) analysis of $\Delta\Psi m$ (TMRM) and mitochondrial mass (EGFP). Ratio between $\Delta\Psi m$ and mitochondrial mass was used to normalize all values for mitochondrial activity. **C-E,** Cell division kinetic was followed by time-lapse microscopy in a microwell system and **C,D,** PDC analysis was performed after TMRM quantification of mitochondrial activity as measured by confocal microscopy. Note that EGFP signal and thus mitochondrial mass does not change upon NR treatment, so all changes in TMRM signal normalized to EGFP reflect changes in $\Delta\Psi m$ and in mitochondrial mass. **E,** PDC analysis on mitochondrial distribution was evaluated in cells treated +/- NR as in C,D and the frequency of cells with highly asymmetric mitochondrial distribution (>Log10) was quantified; *n*=67 and *n*=75. *Student's t test *p<0.05, **p<0.01, ***p<0.001.*

Figure 7. NR improves survival and accelerates blood recovery after HSC transplant.

A, Mice were fed with ctrl or NR-supplemented diet (12mg NR triflate /mouse/day) from 1 week prior to transplantation until the end of all experiments. **B,** Survival of mice transplanted with a limited number of cells ($70*10^5$ total BM cells) was assessed over a period of 40 days, *n=10.* Mantel-Cox ****p<0.001.* **C, D,** Recovery of blood cell counts was assessed over a period of 40 days after transplant of $150*10^5$ total BM cells, *n=10. 2 way ANOVA, Bonferroni post test *p<0.05, **p<0.01, ***p<0.001.* **E,** Wildtype recipient mice were lethally irradiated and transplanted with BM derived from mitoQC mice. Transplanted mice received diet supplemented with NR during throughout the post-transplant recovery period. Mitophagy rate was measured by FACS at 35 days post-transplant in the different hematopoietic progenitor and stem cell compartments. **F,** NSG humanized mice were produced by intrahepatic injection of human CD34+ cells in adult NSG mice. Human CD3+ T lymphocyte levels were assessed in humanized mice after 7 day treatment with control (ctrl) or NR diet (12mg NR /mouse/day). For each mouse the change in % CD3+ cells within the HuCD45+ population following 7d treatment was calculated as fold increase relative to d0, *n=5. Student's t test *p<0.05, **p<0.01, ***p<0.001.* See also Figue S7.

STAR METHODS :

CONTACT FOR REAGENT AND RESOURCE SHARING

Further information and requests for reagents may be directed to and will be fulfilled by the co-corresponding authors olaia.naveiras@epfl.ch (*Lead Contact*) and nicola.vannini@unil.ch.

EXPERIMENTAL MODEL AND SUBJECT DETAILS

Study design

HSC function is strongly regulated by their metabolic state. In this study we aimed to test the modulation of intracellular NAD as a possible strategy to influence HSC fate. In the first part of the study we analyzed the effect of NR on the hematopoietic stem and progenitor compartments. The phenotypic analysis was performed by FACS while functional analysis consisted of CFU colony assay and BM transplantation.

In the second part we evaluated the effect of NR on mitochondrial metabolism. As readout we chose TMRM staining for FACS, a rhodamine based that is absorbed by the mitochondria based on a functional membrane potential, as well as mitochondrial dye MitoTracker Deep Red and JC1 for confocal microscopy. Unfortunately other type of analysis (i.e., proteomics or use of Seahorse metabolic analysers) was not technically possible due to the limited number of cells (LT-HSCs ≈ 1000/mouse and ST-HSCs ≈ 2500/mouse).

In the third part we evaluated the activation of autophagy/mitophagy and mitochondrial stress response as candidate pathways for the reduction in mitochondrial activity. The analysis was performed by RNA sequencing (in vitro NR-treated HSCs) and quantitative RT-PCR (in vivo NR-treated HSCs) in order to assess changes in gene expression for the components of these

pathways. As above, RNA transcription analysis is one of the few methods that allows the analysis of molecular mechanism in such rare populations. Mitonuclear imbalance was validated at the protein level by Western blotting of FACS-sorted LT-HSCs.

In the fourth part we assessed asymmetrical HSC division via confocal microscopy analysis of paired-daughter cells, to evaluate asymmetrical distribution of active mitochondria immediately after cell division.

In the last section we translated our findings to a clinically relevant scenario. Due to the effect of NR on the hematopoietic progenitor compartments, we investigated the capacity of NR to boost blood cell production in post-transplant mice and to improve the survival of mice transplanted with a limited number of BM cells.

Mice

C57Bl/6J and C57Bl/6J Ly5.1 were purchased from Charles River Laboratories International and maintained at the Center for Studying Living System (CAV) at the EPFL in microisolator cages. Mito-QC mice in C57Bl/6J background were provided by P.C. Ho, bred at the Ludwig Institute for Cancer Research Lausanne and their BM analyzed at EPFL. Mito-eGFP mice in C57Bl/6J background ubiquitously expressing enhanced green fluorescent protein (EGFP) in the mitochondria of each cell (R26R/R26-Mito-EGFP) (Abe et al. 2011) were provided by M.P. Lutolf Lab and bred at EPFL. Nrk1-/-;Nrk2-/- mice, also in C57Bl/6 background, were provided by C. Cantó, then bred and analyzed at EPFL. Mice were provided continuously with sterile food, water and bedding. All *in vivo* procedures were carried out in accordance with the Swiss law after approval from the local authorities (Service Vétérinaire de l'Etat de Vaud). All experiments were designed according to the ARRIVE guidelines. NSG mice were purchased from Jackson Laboratory, bred and maintained under pathogen-free conditions

in-house. Animal experimentation followed protocols approved by the Service Vétérinaire de l'Etat de Vaud.

Food preparation

NR diet was prepared by mixing NR triflate (custom synthesized by Novalix, beta form isomer purity > 95%) dissolved in water with 2916 powder diet (Charles River) and air dried into pellets in sterile conditions. The NR dosage in the mix was calculated by taking into account the average mouse food intake per day (5g food/ mouse/ day) for a calculated intake of 12mg NR triflate /mouse/day (=7.57mg/mouse/day of NR+). NA and NAM were provided at the same dose, that is, 480mg/kg of food chow (Cantó et al. 2012). The food was provided ad libitum during the entire period of the experiment. As previously described, food consumption is higher in NR-treated mice in baseline conditions. Food consumption is significantly reduced after BM transplantion; we found no difference in NR versus control food consumption post-transplant. Niagen was purchased from Live Cell Research; NR dose was calculated based on the manufacturer's report of NR chloride content, and capsules were then opened and their full powder content (containing cellulose and silicon dioxide as excipients) was mixed with "2916" powder diet as for custom-synthesized NR triflate.

Murine HSC extraction and culture

Hematopoietic stem cells were isolated from crushed bone marrow of 8- to 12-week old female C57Bl/6J mice. Red blood cells were removed by incubation with a lysis buffer (BioLegend). Lineage positive cells were eliminated using a magnetic lineage depletion kit (Miltenya Biotech). Cells in suspension were stained with SAV-PO or SAV-TxRed, Kit-PE-CY7, Sca1-PE, CD150-BV784 or CD150-PE or CD150-PE-CY5, CD48-PB, CD34-eF660 or CD34-FITC and FACs-sorted using a FACSAria II, FACSAria Fusion (BD) or MoFlo Astrios (Beckman Coulter) cell

sorter. LT-HSC compartment was defined as Lin− C-kit+ Sca1+ CD150+ CD48− CD34−. ST-HSC compartment was defined as Lin− C-kit+ Sca1+ CD150+ CD48− CD34+. MMP compartment was defined as Lin− C-kit+ Sca1+ CD150−. CP compartment was defined as Lin− C-kit+ Sca1−. MEP compartment was defined as Lin− C-kit+ Sca1+ CD150−. CP compartment was defined as Lin− C-kit+ Sca1−. MEP compartment was defined as Lin− C-kit+ Sca1− CD34−.

HSCs were sorted and cultured for 2 or 5 days. Cultures were maintained in Stemline II (Sigma) supplemented with 100ng/ml SCF (R&D) and 2ng/ml Flt3 (R&D), +/ - 500μM NR or increasing concentrations up to 2mM for the dose-response curves. NR and NMN were replenished every 24h (2 day cultures) or 48h (5 day cultures) into the culture media.

Human hematopoietic cells

Cord blood, fetal liver and adult bone marrow (hip replacement surgery) came from consent donors. Collection and experimental procedures were carried out in accordance with the Swiss law after approval from the pertinent local authorities: Swiss Ethics Commissions on research involving humans (Vaud canton protocol number VD2797 and 336/1 to G.C. for fetal liver, CER-VD2017-00846 to O.N. for adult bone marrow, and Zurich canton protocol number Stv22/2006 to M.E. for non-commercial cord blood). Human CD34+ cord blood were alternatively purified from a cord blood bag provided by the “Etablissement de Transfusion Sanguine Bourgogne Franche-Comté” (Besançon).

In vitro culture of human CD34+ hematopoietic progenitor/stem cells

Human CD34+ cells were isolated from fetal liver, cord blood or adult bone marrow by human CD34 positive selection (StemCell Technologies #18056), then cultured either directly after isolation or after cryopreservation in StemSpan media (StemCell Technologies, #09600)

supplemented with SCF (100ng/ml), FLT3L (100ng/ml), TPO (50ng/ml), LDLP (10ug/ml) and different concentrations of NR. Each well of a 96-round-well plate contained 90,000 CD34+ progenitors in 200 µl of media. The culture media was supplemented with fresh NR every 24 hours. After the indicated culture period the cells were stained, washed and analyzed by flow cytometry.

Murine bone marrow transplantation

C57Bl/6 Ly5.2 mice were lethally irradiated with a total 850 rad dose in a X-ray radiator (RS-2000, RAD SOURCE) 24h before transplant. The dose was split in two doses of 425 rads separated by a 4-hour interval. Mice were injected with donor cells derived from C57Bl/6 Ly5.1 mice and competitor cells derived from C57Bl/6 Ly5.1/5.2 mice, via tail-vein injection. For the 7-day NR treatment, donors received $150*10^3$ total BM donor cells together with $150*10^3$ total BM competitor cells. For at least two weeks after lethal irradiation mice were treated with paracetamol and antibiotics in the form of either Bactrim for the limiting-dose transplantation studies (Sulfa and TMP 60mg/Kg/day: 250ml of water with 2.5ml of Bactrim (200mg Sulfa /40mg TMP)) or Baytril/Co-amoxiciline (300 ul of Baytril 10% solution plus 2.5 ml of Amoxymepha to 250 ml of drinking water) for all other transplants. Peripheral blood was collected at 1,2 and 4 months to determine the percentage of chimerism by FACS analysis. For the limiting transplant experiments, mice received $75*10^3$ total BM donor cells and the health status of the animals was monitored twice daily. For the blood recovery curves mice were transplanted with$150*10^3$ total BM donor cells. Blood was collected twice per week (blood volume 50 microliters) and analyzed by standard veterinarian blood cell counter (ABC^{tm}).

Transplantation of human CD34+ hematopoietic progenitor/stem cells

For transplantation, one day old NSG pups were irradiated with 1Gy and few hours later injected intrahepatically with in vitro expanded hCD34+ HSPCs. Each pup was injected with a cell mass containing 50,000 CD34+ cells after thawing and *in vitro* culture. Mice were bled, via tail vein, every 4 weeks, starting from 8 weeks until 36 weeks to quantify human reconstitution levels (% human CD45+ cells) in the peripheral blood. Antibody combinations were used to further estimate human B cells, T cells, Monocytes, Neutrophils and NK cells. At the endpoint (36 weeks), BM and spleen were isolated to determine the level of human reconstitution at these two sites.

For secondary transplantation, adult (8-10 weeks) NSG mice were irradiated with 2Gy and one day later injected intravenously with bone marrow cells isolated from primary recipients. Bone marrow from each primary recipient was injected in 3 secondary recipients (8 million cells per mouse). Mice were bled, via tail vein, every 4 weeks, starting from 8 weeks until 24 weeks to estimate human reconstitution levels (% human CD45+ cells) in peripheral blood. Antibody combinations were used to further estimate human B cells, T cells, Monocytes, Neutrophils and NK cells. At the endpoint (24 weeks), bone marrow and spleen were isolated to determine the level of human reconstitution at these two sites.

Flow cytometry

Flow cytometry analysis of stem and progenitor hematopoietic compartments was performed on freshly isolated bone marrow (BM). BM was extracted from crushed femora and tibia. Cells suspension was filtered through 70μm cell strainer and erythroid cells were eliminated by incubation with red blood cells lysis buffer (eBioscences). Isolation and stains were performed in ice-cold PBS 1mM EDTA. Lineage positive cells were then removed with a magnetic lineage depletion kit (Milteny Biotechnology). Cells suspension were then stained with specific

antibodies for stem/progenitor compartments and analyzed or sorted respectively on BD LSR2 and BD FACS Aria 2.

Analysis of mitochondrial activity

Freshly isolated BM cells were incubated at 37°C for 1 hour with 200nM TMRM (Invitrogen) and subsequently stained with specific antibodies for different hematopoietic compartments. Cells were then analyzed or sorted by flow cytometry. For confocal imaging, LT-HSC and ST-HSC were sorted into StemLine II supplemented with SCF+Flt3L +/- NR as for HSC culture, and let adhere on a poly-lysine coated slide for 6 hour. JC-1 was then added in the cell media according to the manufacturer instructions (Cayman Chemical) and live cell images were acquired on a Leica SP5.

Analysis of autophagy flux

Sorted LT and ST cells were cultured in complete growth medium in presence or absence of ±500µM NR for 24hours and treated with 5nM Bafilomycin or PBS for additional 12 hours. The cells were treated with Mitotracker Deep Red (Thermo Scientific), fixed with PFA 4%, stained for Lc3b (Cell Signaling) and mounted using Prolong mounting medium with DAPI (Thermo Scientific). For Lc3b, we used donkey anti-rabbit 555 secondary antibody (Alexa). The fluorescent pictures were taken using Zeiss 880LSM Airyscan. 3D whole cell reconstructions were analyzed using Imaris software (Bitplane) to calculate Lc3b punctae number and mitochondria surface, utilizing dot and surface analyses functions.

CFUs assay

12500 total bone marrow cells were isolated from the legs and hips of C57Bl/6J mice and cultured in MethoCult (StemCell technology) containing recombinant SCF, EPO, IL-3 and IL-6.

Number and morphology of the colonies were analyzed with phase contrast microscope after 7 days of culture.

CFSE

Freshly sorted LT-HSCs were incubated for 20 min at 37°C with 1:400 CFSE stock solution (Cayman chemicals; CFSE cell division assay kit). The cells were pelleted and re-suspended in 1ml of Stemline II (Sigma) containing 10% FBS for 20 min at 37°C. Thereafter, the cells were washed twice with 1ml of Stemline II (Sigma) and put in culture as described above. KLSCD150- cells were sorted with LT- and ST-HSCs and, given their higher frequency and higher proliferative state, used as controls for determining the peaks of CFSE intensity corresponding to 0 and 1 divisions.

Seahorse Oxygen Respiration Rate (OCR) measurement

OT-1 splenocytes were stimulated in vitro with SIINFEKL peptide and IL-2 for in the presence of NR or Ctrl treatment. Cells were plated at equivalent cell number, and ECAR and OCR measurements were assayed upon stimulation in the Seahorse XF24 bioanalyzer (Seahorse Bioscience). Cells were washed and resuspended in serum-free unbuffered KHB medium containing 25mM Glucose, 2mM Glutamine, 1mM pyruvate, 150μM Oleate and 1.5mM Carnitine. The cells were then were plated onto Seahorse cell plates (4×10^5 cells per well) coated with Cell-Tak (BD Bioscience) to allow their attachment. Perturbation profiling of substrate was achieved by addition of oligomycin (1 μg/ml), FCCP (1.5 μM), Etomoxir (200μM), rotenone (100nM) and Antimycin A (1μM; all from Sigma-Aldrich). Experiments with the Seahorse apparatus were done with the following assay conditions: 2-3 min mixture; 2 minutes wait; and 3-4 min measurement.

RNA preparation

LT-HSC and ST-HSCs were FACS sorted (>10^4cells per sample), cultured for two days in presence or absence of NR as indicated above, then resuspended in RNA lysis buffer (Zymo Research) and total RNAs extracted using the Quick-RNA Microprep Kit (R1050, Zymo Reseach) following the manufacturer's instructions. The extraction included a DNA-digestion step and was finally reconstituted in 12.5 µl ddH2O. In parallel, and as a quality control, some cells were stained with TMRM and analyzed by flow cytometry to verify a significant decrease in ΔΨm upon NR-treatment.

Total RNA content was quantified using the Qubit 3 Fluorometer (Invitrogen), and RNA quality control was performed by profile analysis on a TapeStation 4200 system (Agilent) following the manufacturer's protocol. The cDNAs were prepared from 2.5 ng RNA per sample with the "SMART-seq v4 Ultra Low Input RNA Kit for Sequencing" (Clontech), and subsequently processed into sequencing libraries with the Nextera XT kit (Illumina FC-131-1096), in both cases following manufacturer's instructions. The resulting libraries were quantified using a Qubit 3 Fluorometer and their profile monitored on a TapeStation 4200 system.

RNA-seq

Sequencing was performed on a NextSeq 500 system (Illumina) using a High Output cartridge with up to $4*10^8$ Single-End 75 nt reads , following manufacturer's instructions.

The fastq files were evaluated using FastQC v0.11.2 and aligned to the Ensembl-91 gene annotation of GRCm81 using STAR v2.5.0b. The number of tags belonging to each gene was then counted using HTSeq v0.6.1 with the following parameters "htseq-count -s no -m union -f bam". A good quality of mapping was reached since a sufficient proportion of reads (from 60%

to 80%) were uniquely mapped to exonic regions. Raw counts for each gene were expressed in counts per million (cpm) for filtering. Only genes expressed in at least three samples with a cpm greater than 0.5 were kept for the rest of the analysis, resulting in a filtered data set of 14034 genes expressed across 12 samples. After this step the 6 replicates (3 control and 3 NR treated, corresponding to three separate FACS isolation and culture batches) for LT or ST-HSCs were processed separately. As a first step the raw counts were normalized using VOOM from Limma v3.34.9 and corrected for batch effect using ComBat. NR-treatment became significantly correlated with the first principal component (PC) of the PC analysis. At this stage, the batches were not significant anymore, meaning that the batch correction was successful. The differentially expression analysis between NR treated cells versus control was performed using Limma pipeline with a cutoff of 2-Fold increase and FDR > 0.05. Finally, we used Gene Set Enrichment Analysis (GSEA software from Broad Institute v3.0) to determine whether some specific gene sets revealed significant difference upon NR treatment. We tested five gene sets defined in the Gene Ontology Consortium: Autophagy (GO:0006914), Oxidative Phosphorylation (GO:0006119), Fatty acid oxidation (GO:0019395), Tricarboxylic Acid Cycle (GO:0006099) and Mitophagy (GO:000423) as well as two manually defined genes sets, since they were not defined by any GO term: NAD salvage and *de novo* synthesis pathway (*Nmnat1, Nmnat2, Nmnat3, Nampt, Nmrk1, Nmrk2, Naprt, Nadsyn1, Tdo2, Afmid, Kmo, Kynu, Haao, Qprt and Ido1*) from (Bogan KL and Brenner C, 2008) and mitochondrial unfolded protein response (*Hsp60, mt-Hsp70, Hsp10, ClpP, Lonp1, Jnk2, c-Jun, Chop, Cebp-beta, Yme1l1, Afg3l2, Spg7, Sirt1 and Ubl5*; from Jovaisaite V. and Auwerx J. ,2015; D'Amico D et al., 2017).

The differences between the means of the conditions were used to calculate the fold changes and the enrichment score was estimated using the weighted statistical approach and evaluated for significance by doing 20000 genes set based permutations.

Q-RT-PCR

1,000-50,000 LT-HSCs and ST-HSCs were sorted directly in lysis buffer from ZR RNA MicroPrep (Zymo Research) and RNA extraction was performed accordingly to the manufacturer instructions. RNA was eluted and re-suspended in 6µl of H_2O. 2µl of RNA was retro-transcribed to cDNA with Vilo Script system (Invitrogen). Subsequently cDNA was diluted 5 times in water. For QPCR 1.5µl of cDNA, 5µl of *Power* Syber Green mastermix (Applied Biosystem) and 200nM of primers were used to a final volume of 10µl for each reaction. The reactions were performed on the 7900HT system (Applied Biosystem).
Gene expression was normalized to *Arbp* as housekeeping control. Amplification of the template at more than 40 cycles (Ct>40) was considered as indeterminate expression of the gene of interest.

Western blotting

For murine mitonuclear imbalance assessment, 30,000 LT- or 30,000 ST-HSCs were FACS sorted from Lineage depleted bone marrow from 32 mice after 7 day NR- or control diet treatment. Cells were directly sorted in urea lysis buffer [20 mM HEPES pH 8, 9 M Urea, 1 mM sodium orthovanadate, 2.5 mM sodium pyrophosphate, 1 mM β-glycerophosphate, and 1X protease inhibitor cocktail (Roche)]. Proteins were separated by SDS-PAGE and transferred to a PVDF membrane (0.45 µm). Blocking and antibody incubations were performed in 3% BSA in

Tris-buffered saline with Tween 20 (TBS-T). The following primary antibodies were used against MTCO1 (Abcam, ab14705) and ATP5A (abcam, ab14748).

For mitonuclear imbalance assessment in human cells, K562 cells were cultured with RPMI 10% FCS 1% Penicillin/Streptomycin in 96 well plates. K562 cells were then treated with NR in a dose-response for 2 days, with a replenishment dose after 24h. Total cell lysates were prepared using a lysis buffer [20 mM Tris-HCl (pH7.5), 150 mM NaCl, 1 mM EDTA, 1 mM EGTA, 1% Triton X-100, 2.5 mM Sodium pyrophosphate, 1 mM β-Glycerrophosphate, and 1X protease inhibitor cocktail (Thermo, Cat. 78430)], proteins were then normalized by a DC protein assay (BIO-RAD, Cat. 500-0116). Western blotting was performed with antibodies against MTCO1 (Abcam, ab14705), SDHA (Abcam, ab14715), ATP5A (abcam, ab14748), HSP60 (Santa Cruz, sc-1052).

Hydrogel microwell array production and single cell cycle kinetics

Hydrogel microwell arrays were directly casted within individual wells of a 96-well plate as described (Kobel et al., 2009). Briefly, stoichiometrically balanced aqueous solutions of multi-arm poly(ethylene glycol) (PEG), end-functionalized with thiol and vinylsulfone groups were mixed and molded against a PDMS microstamp. Upon completion of crosslinking, the stamp was removed and the hydrogel microwell array was hydrated overnight at 4 °C and then sterilized with ultraviolet light. To follow the behavior of HSCs at single cell level, cells were sorted directly into 96-well plates coated with microwell arrays. Microwells containing a single cell at the time of plating were tracked by time-lapse microscopy. Cells were cultured in basal medium (Stemline II containing 2ng/ml Flt3 and 100ng/ml SCF) supplemented with or without 500μM NR. Proliferation kinetics were assessed using a Zeiss Axio Observer microscope equipped with an incubator chamber, temperature and CO_2 control. Images were automatically

acquired every three hours over five days using the imaging analysis software of MetaMorph (Visitron, Germany).

Imaging and analysis for asymmetric divisions

Freshly isolated LT-HSCs were directly seeded onto a platform containing rectangular cavities (grooves) enabling single cell tracking during culture. The platform was immersed in serum free medium (Sigma-Aldrich, St. Louis, USA) supplemented with 100ng/ml stem cell factor (SCF) and 2ng/ml Flt-3 ligand (R&D Systems, Minneapolis, USA). To track precisely each cells, brightfield images were acquired every 30mn. After 35 hours of culture, TMRM was added to a final concentration of 20nM. Mitochondrial mass and potential were acquired by performing z-stacking on live cells on a Visitron CSU-W1 microscope. Paired-daughter cells asymmetry was quantified as the difference of their respective potential normalized by their mitochondrial mass (intensity thresholded TMRM signal divided by thresholded EGFP signal).

***In vivo* NR treatment of adult humanized NSG mice**

Cryopreserved mobilized CD34+ cells from healthy donors (purified CD34+ from mobilized blood, Cellsystems Biotechnologie GmbH, Troisdorf, DE or STEMCELL Technologies, SARL) were thawed and used immediately for transplantation.

NSG mice were purchased from The Jackson Laboratory and bred, treated, and maintained under pathogen-free conditions in-house. Animal experimentation followed protocols approved by the Service Vétérinaire de l'Etat de Vaud. Nine to ten week-old NSG mice were irradiated with 1.8Gy and 6 hours later injected intravenously with 10^6 human CD34+ HSC (purified CD34+ from mobilized blood, Cellsystems Biotechnologie GmbH, Troisdorf, DE or STEMCELL Technologies, SARL). The level of human reconstitution (% human CD45+ cells) was analyzed 12 weeks later by FACS staining of tail vein blood samples. Mice were regrouped based on level

of reconstitution into two comparable cohorts of 5 mice each. The following day and for a total of 7 days, cohorts received 2916 powder chow diet supplemented or not with NR, as for C57BL/6 mice. After 7 days tail vein blood was collected in EDTA tubes and mice sacrificed for BM analysis. BM cells were collected as described for C57BL/6 mice, and both blood and BM cells stained and analyzed for a panel of human lineage specific antibodies as described above.

QUANTIFICATION AND STATISTICAL ANALYSIS

Statistics

Data were statistically analyzed by Student's t test, one and two way ANOVA as specified in each figure legend with Prism GraphPad software. The modified Z Score was used to test for outliers.

DATA AND SOFTWARE AVAILABILITY

Primary data is accessible in Mendeley Data with repository number: (awaiting link). The RNAseq data discussed in this publication have been deposited in NCBI's Gene Expression Omnibus (Edgar et al., 2002) and are accessible through GEO Series accession number GSE125211 (http://www.ncbi.nlm.nih.gov/geo/query/acc.cgi?acc=GSE125211).

STAR METHODS REFERENCES

Edgar, R., M. Domrachev and A.E. Lash (2002). Gene Expression Omnibus: NCBI gene expression and hybridization array data repository. *Nucleic Acids Res* **30**(1):207-10 .

Figure 1

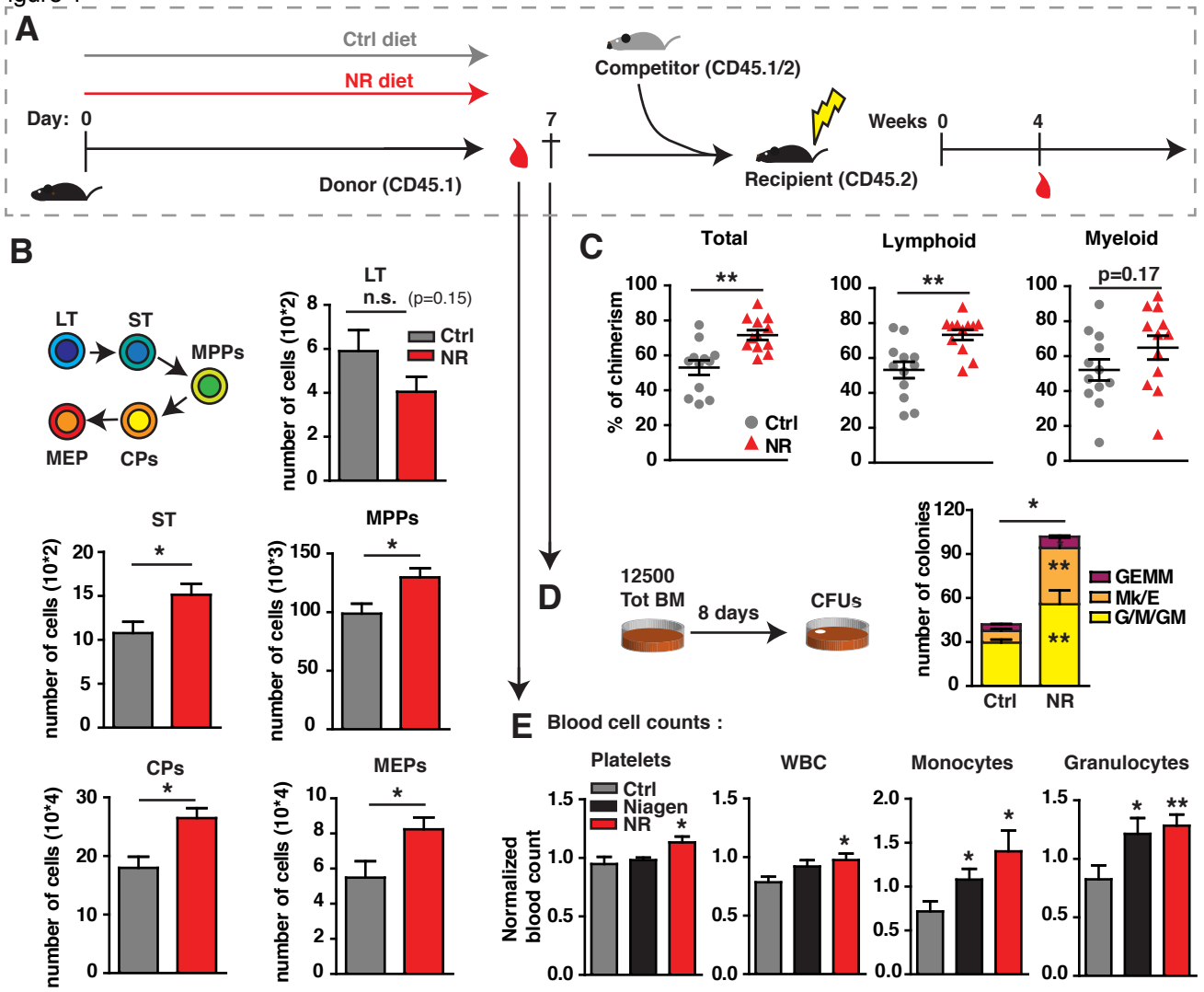
A
Ctrl diet
NR diet
Day: 0
7
Donor (CD45.1)
Competitor (CD45.1/2)
Recipient (CD45.2)
Weeks 0
4
B
LT
ST
MPPs
MEP
CPs
LT
n.s. (p=0.15)
Ctrl
NR
number of cells (10*2)
ST
number of cells (10*2)
MPPs
number of cells (10*3)
CPs
number of cells (10*4)
MEPs
number of cells (10*4)
C
Total
Lymphoid
Myeloid
% of chimerism
p=0.17
Ctrl
NR
D
12500
Tot BM
8 days
CFUs
number of colonies
GEMM
Mk/E
G/M/GM
Ctrl
NR
E
Blood cell counts :
Platelets
WBC
Monocytes
Granulocytes
Ctrl
Niagen
NR
Normalized blood count

Figure 2

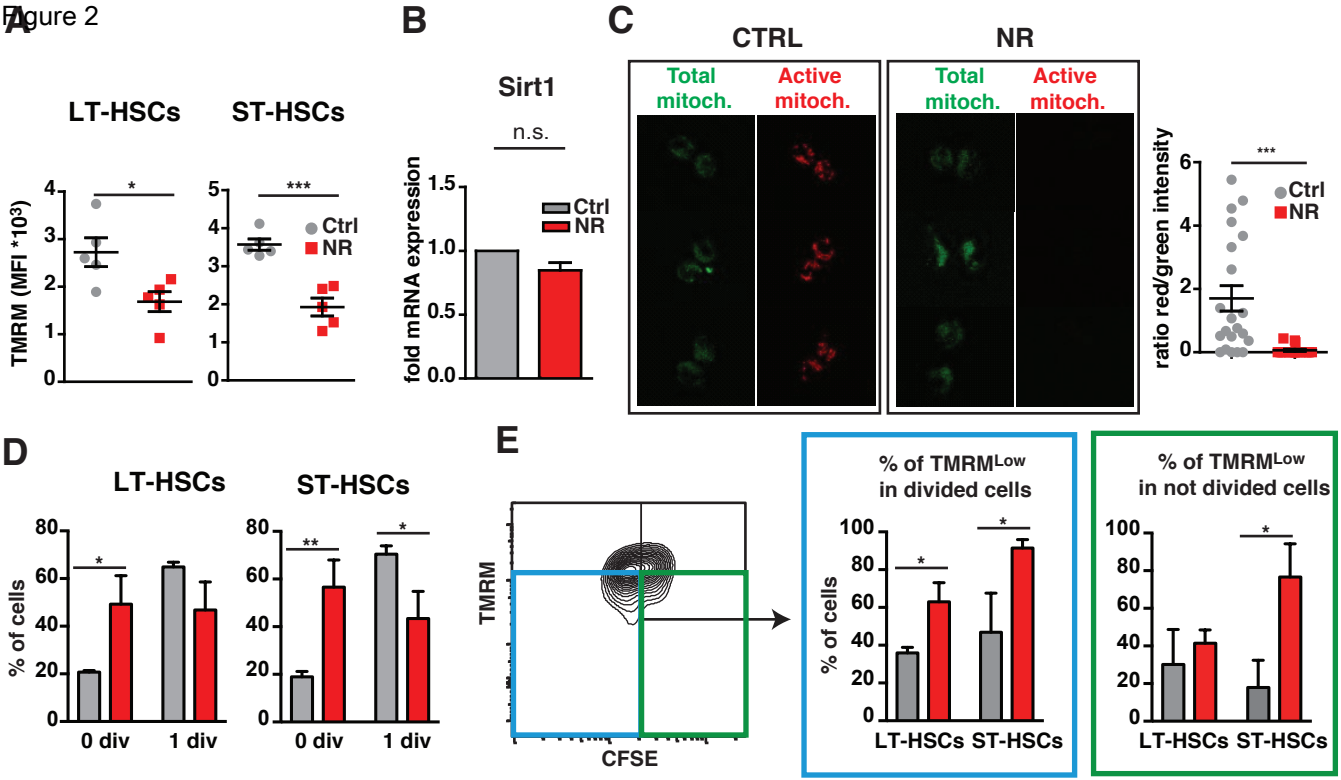
A
LT-HSCs
ST-HSCs
TMRM (MFI *10³)
Ctrl
NR
B
Sirt1
n.s.
fold mRNA expression
C
CTRL
NR
Total mitoch.
Active mitoch.
ratio red/green intensity
D
LT-HSCs
ST-HSCs
% of cells
0 div
1 div
E
TMRM
CFSE
% of TMRMLow in divided cells
% of TMRMLow in not divided cells
LT-HSCs
ST-HSCs

Figure 3

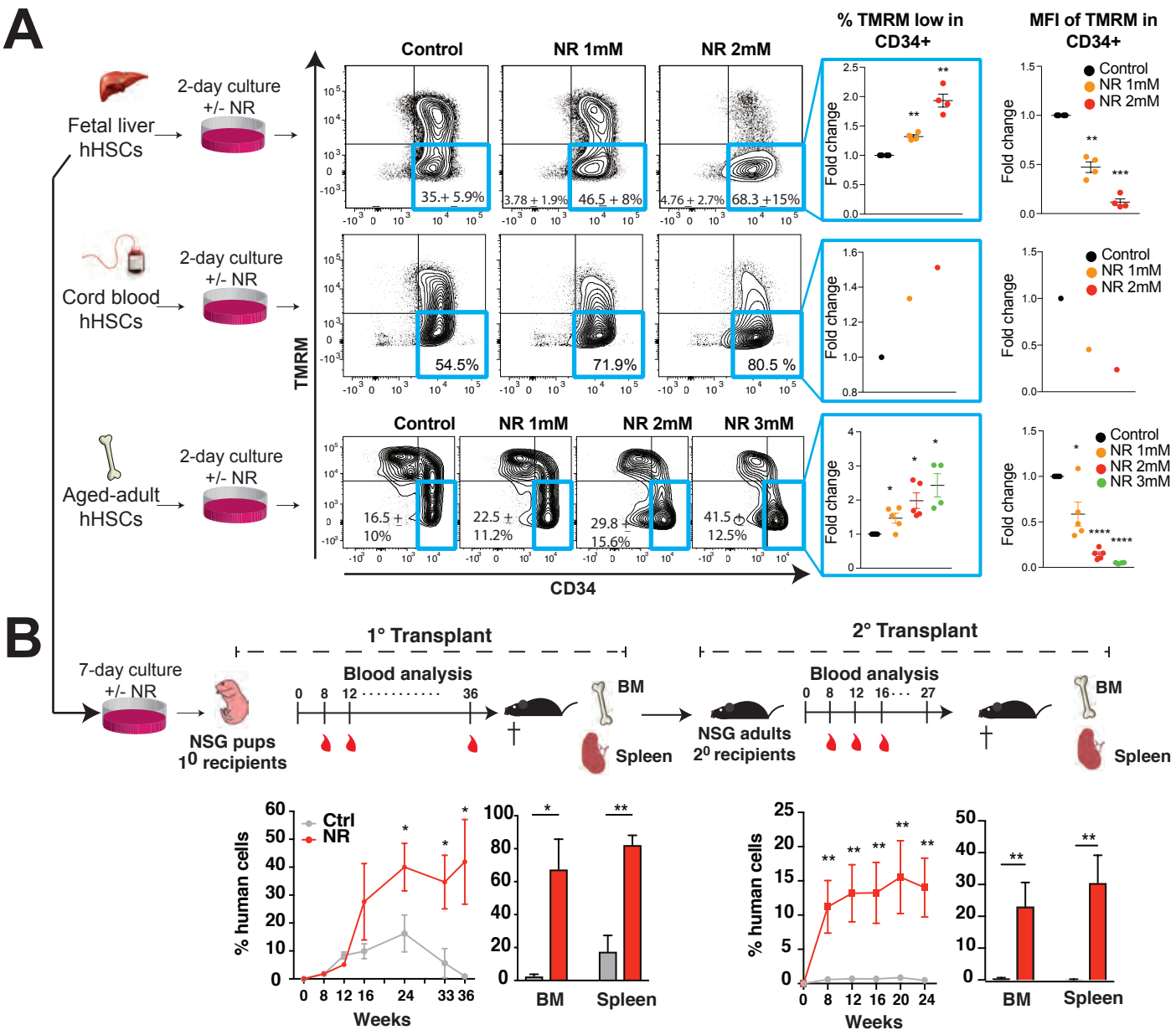
A
Fetal liver hHSCs
2-day culture +/- NR
Cord blood hHSCs
2-day culture +/- NR
Aged-adult hHSCs
2-day culture +/- NR
Control
NR 1mM
NR 2mM
NR 3mM
TMRM
CD34
35.+ 5.9%
3.78 + 1.9%
46.5 + 8%
4.76 + 2.7%
68.3 +15%
54.5%
71.9%
80.5 %
16.5 + 10%
22.5 + 11.2%
29.8 + 15.6%
41.5 + 12.5%
% TMRM low in CD34+
MFI of TMRM in CD34+
Fold change
B
7-day culture +/- NR
NSG pups 10 recipients
1° Transplant
Blood analysis
BM
Spleen
NSG adults 20 recipients
2° Transplant
% human cells
Ctrl
NR
Weeks

Figure 4

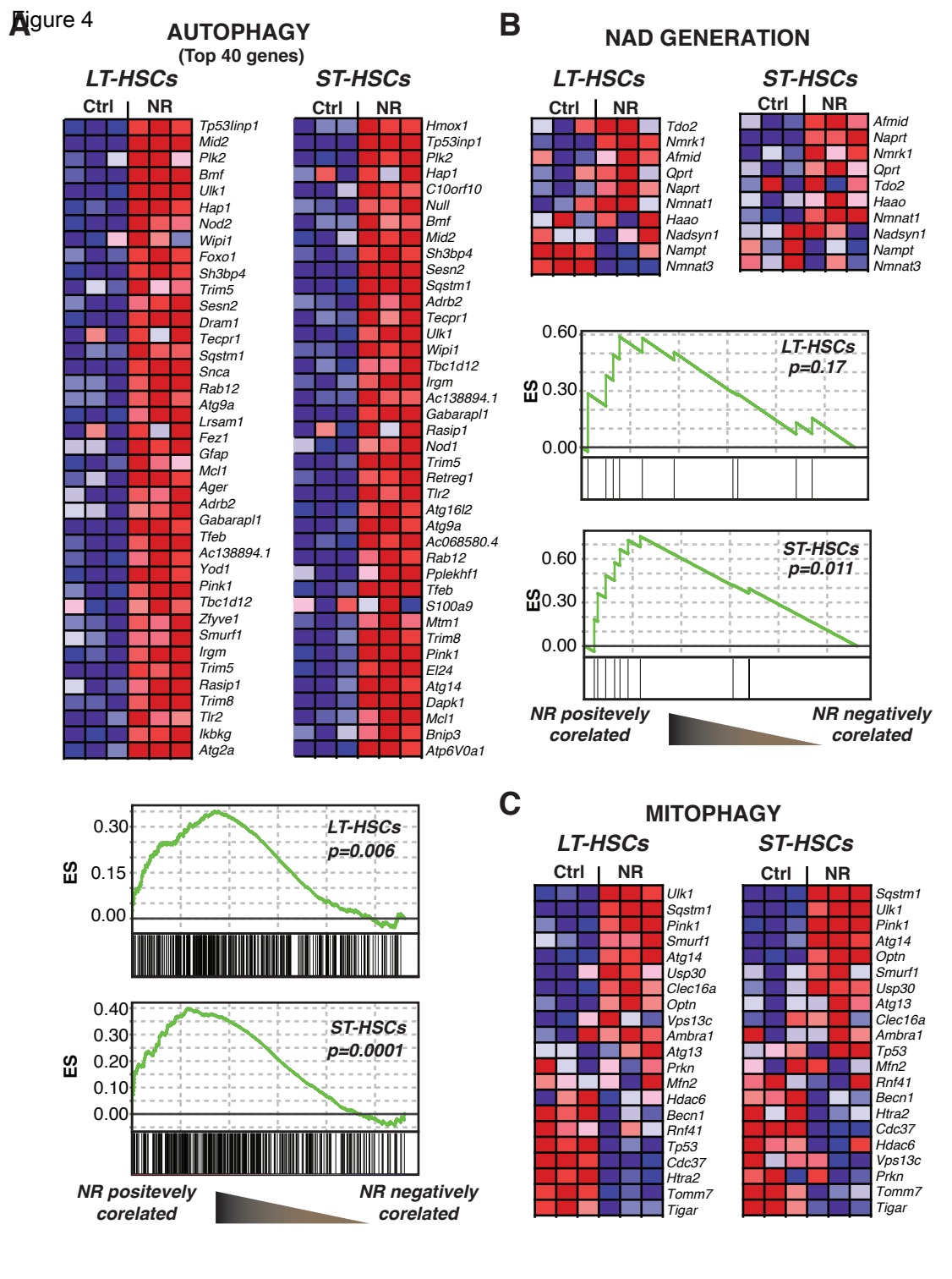
A
AUTOPHAGY
(Top 40 genes)
LT-HSCs
ST-HSCs
Ctrl
NR
Tp53linp1
Mid2
Plk2
Bmf
Ulk1
Hap1
Nod2
Wipi1
Foxo1
Sh3bp4
Trim5
Sesn2
Dram1
Tecpr1
Sqstm1
Snca
Rab12
Atg9a
Lrsam1
Fez1
Gfap
Mcl1
Ager
Adrb2
Gabarapl1
Tfeb
Ac138894.1
Yod1
Pink1
Tbc1d12
Zfyve1
Smurf1
Irgm
Trim5
Rasip1
Trim8
Tlr2
Ikbkg
Atg2a
Hmox1
Tp53inp1
Plk2
Hap1
C10orf10
Null
Bmf
Mid2
Sh3bp4
Sesn2
Sqstm1
Adrb2
Tecpr1
Ulk1
Wipi1
Tbc1d12
Irgm
Ac138894.1
Gabarapl1
Rasip1
Nod1
Trim5
Retreg1
Tlr2
Atg16l2
Atg9a
Ac068580.4
Rab12
Pplekhf1
Tfeb
S100a9
Mtm1
Trim8
Pink1
El24
Atg14
Dapk1
Mcl1
Bnip3
Atp6V0a1
B
NAD GENERATION
LT-HSCs
ST-HSCs
Ctrl
NR
Tdo2
Nmrk1
Afmid
Qprt
Naprt
Nmnat1
Haao
Nadsyn1
Nampt
Nmnat3
Afmid
Naprt
Nmrk1
Qprt
Tdo2
Haao
Nmnat1
Nadsyn1
Nampt
Nmnat3
ES
0.60
0.30
0.00
LT-HSCs
p=0.17
ES
0.60
0.30
0.00
ST-HSCs
p=0.011
NR positevely
corelated
NR negatively
corelated
C
MITOPHAGY
LT-HSCs
ST-HSCs
Ctrl
NR
Ulk1
Sqstm1
Pink1
Smurf1
Atg14
Usp30
Clec16a
Optn
Vps13c
Ambra1
Atg13
Prkn
Mfn2
Hdac6
Becn1
Rnf41
Tp53
Cdc37
Htra2
Tomm7
Tigar
Sqstm1
Ulk1
Pink1
Atg14
Optn
Smurf1
Usp30
Atg13
Clec16a
Ambra1
Tp53
Mfn2
Rnf41
Becn1
Htra2
Cdc37
Hdac6
Vps13c
Prkn
Tomm7
Tigar
ES
0.30
0.15
0.00
LT-HSCs
p=0.006
ES
0.40
0.30
0.20
0.10
0.00
ST-HSCs
p=0.0001
NR positevely
corelated
NR negatively
corelated

Figure 5

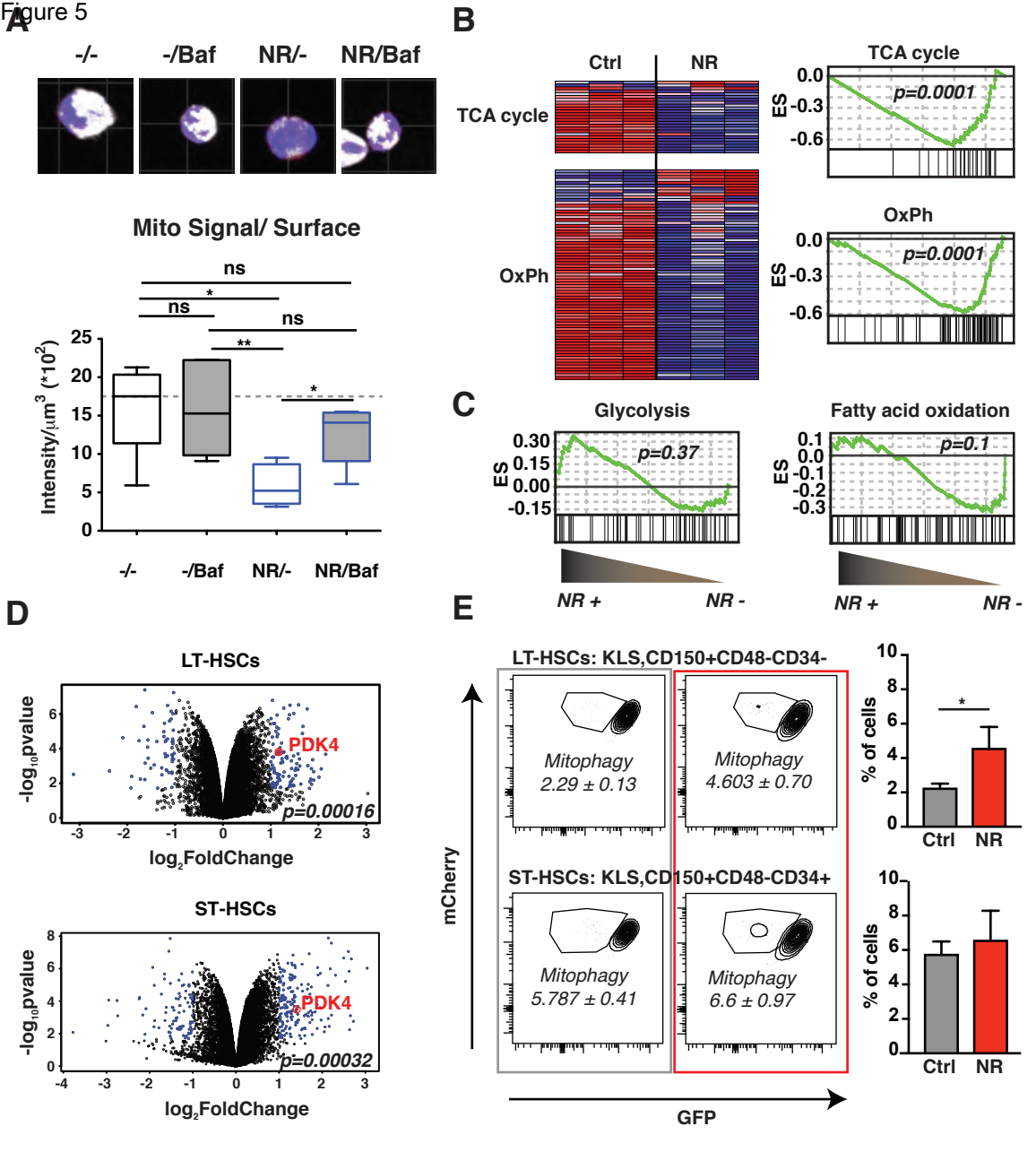
A
-/-
-/Baf
NR/-
NR/Baf
Mito Signal/ Surface
ns
*
ns
ns
**
*
Intensity/μm3 (*10^2)
25
20
15
10
5
0
-/-
-/Baf
NR/-
NR/Baf
B
Ctrl
NR
TCA cycle
OxPh
TCA cycle
p=0.0001
ES
0.0
-0.3
-0.6
OxPh
p=0.0001
C
Glycolysis
p=0.37
0.30
0.15
0.00
-0.15
NR +
NR -
Fatty acid oxidation
p=0.1
0.1
0.0
-0.1
-0.2
-0.3
D
LT-HSCs
-log10pvalue
PDK4
p=0.00016
log2FoldChange
ST-HSCs
PDK4
p=0.00032
E
LT-HSCs: KLS,CD150+CD48-CD34-
Mitophagy
2.29 ± 0.13
Mitophagy
4.603 ± 0.70
ST-HSCs: KLS,CD150+CD48-CD34+
Mitophagy
5.787 ± 0.41
Mitophagy
6.6 ± 0.97
mCherry
GFP
% of cells
Ctrl
NR

Figure 6

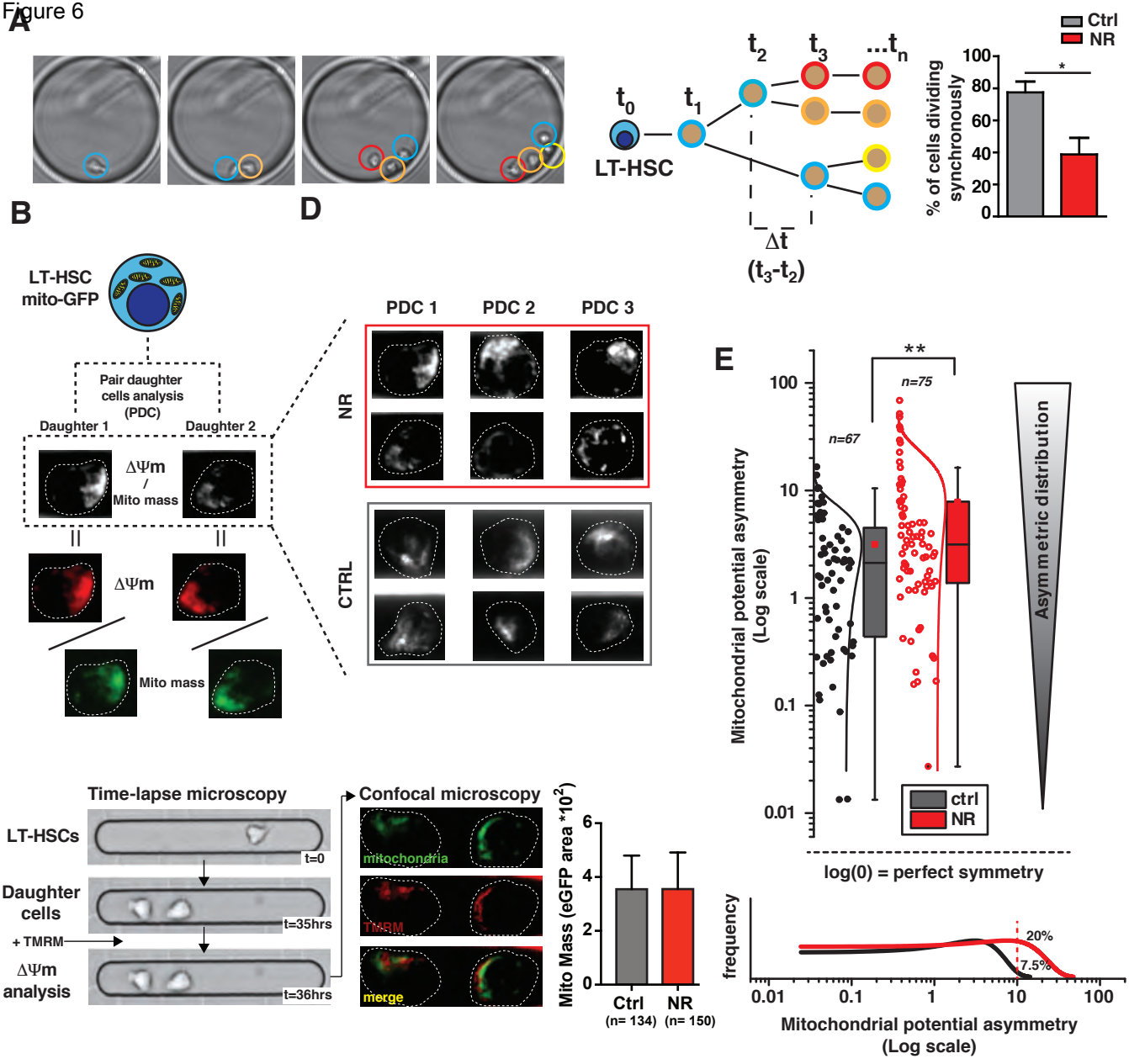
A
t0
t1
t2
t3
...tn
LT-HSC
Δt
(t3-t2)
Ctrl
NR
% of cells dividing synchronously
100
80
60
40
20
0
*
B
LT-HSC mito-GFP
Pair daughter cells analysis (PDC)
Daughter 1
Daughter 2
ΔΨm / Mito mass
ΔΨm
Mito mass
D
PDC 1
PDC 2
PDC 3
NR
CTRL
E
**
n=67
n=75
Mitochondrial potential asymmetry (Log scale)
100
10
1
0.1
0.01
Asymmetric distribution
ctrl
NR
log(0) = perfect symmetry
frequency
20%
7.5%
0.01
0.1
1
10
100
Mitochondrial potential asymmetry (Log scale)
Time-lapse microscopy
LT-HSCs
t=0
Daughter cells
t=35hrs
+ TMRM
ΔΨm analysis
t=36hrs
Confocal microscopy
mitochondria
TMRM
merge
Mito Mass (eGFP area *10^2)
6
4
2
0
Ctrl
(n= 134)
NR
(n= 150)

Figure 7

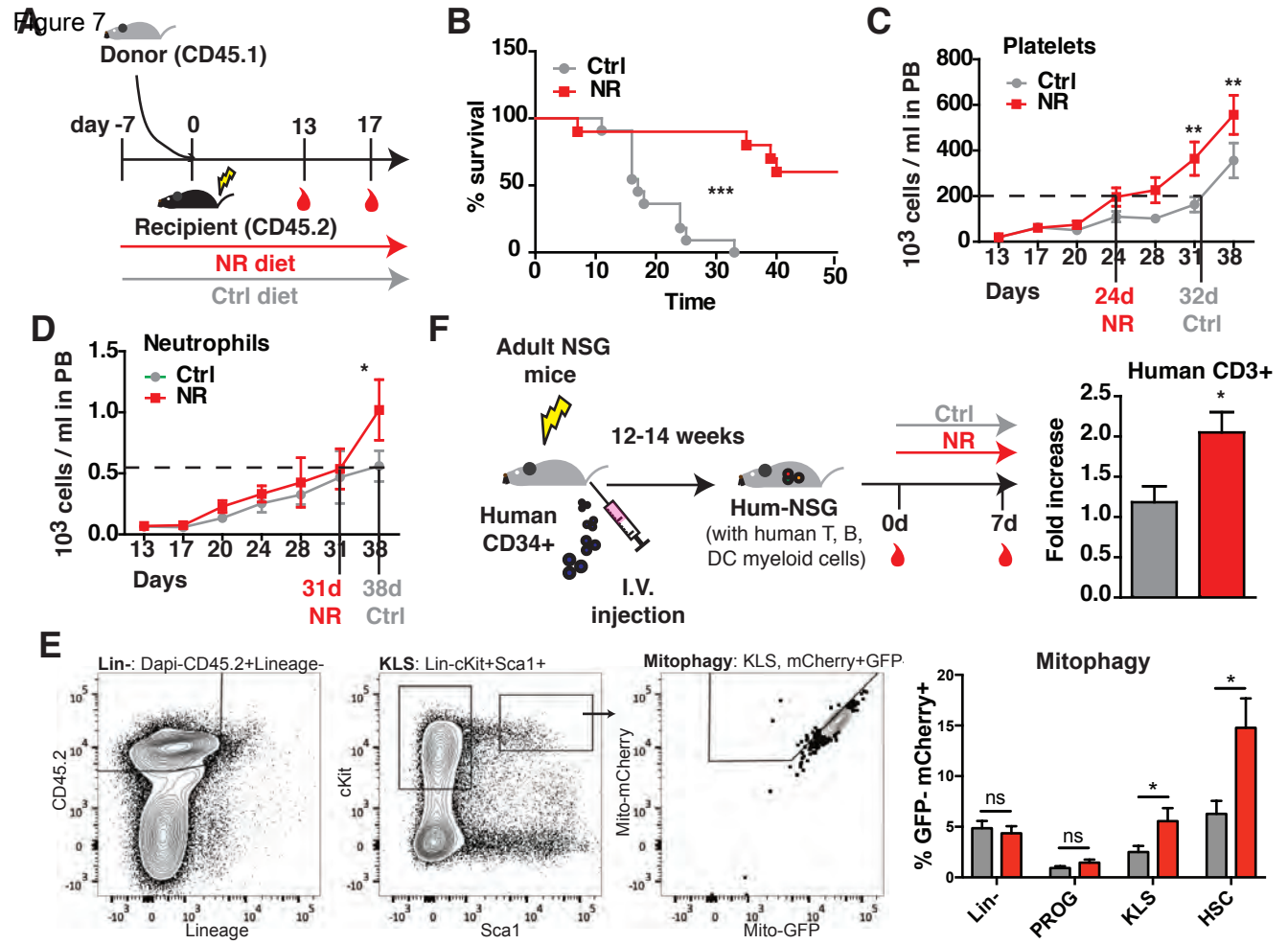
A
Donor (CD45.1)
day -7
0
13
17
Recipient (CD45.2)
NR diet
Ctrl diet
B
% survival
Ctrl
NR
***
Time
C
Platelets
10^3 cells / ml in PB
Ctrl
NR
**
**
Days
24d NR
32d Ctrl
D
Neutrophils
10^3 cells / ml in PB
Ctrl
NR
*
Days
31d NR
38d Ctrl
F
Adult NSG mice
12-14 weeks
Human CD34+
I.V. injection
Hum-NSG
(with human T, B, DC myeloid cells)
Ctrl
NR
0d
7d
Human CD3+
Fold increase
*
E
Lin-: Dapi-CD45.2+Lineage-
CD45.2
Lineage
KLS: Lin-cKit+Sca1+
cKit
Sca1
Mitophagy: KLS, mCherry+GFP-
Mito-mCherry
Mito-GFP
Mitophagy
% GFP- mCherry+
ns
ns
*
*
Lin-
PROG
KLS
HSC

Title: The NAD-booster nicotinamide riboside potently stimulates hematopoiesis through increased mitochondrial clearance

Authors:
N. Vannini[1,2]*‡, V. Campos[1]*, M. Girotra[2,3], V. Trachsel[3], S. Rojas-Sutterlin[1], J. Tratwal[1], S. Ragusa[2], E. Stefanidis[2,4], D. Ryu[5]†, P.Y. Rainer[6], G. Nikitin[3], S. Giger[3], Y.L. Terytty[5], A. Semilietof[2,4], A. Oggier[1], Y. Yersin[1], L. Tauzin[7], E. Pirinen[5]†, W.C. Cheng[2], J. Ratajczak[8], C. Canto[8,9], M. Ehrbar[10], F. Sizzano[8], T.V. Petrova[2,11], D.Vanhecke[2], L. Zhang[2]†, P. Romero[2], A. Nahimana[12], S. Cherix[13], M.A. Duchosal[12], P.C. Ho[2], B. Deplancke[6], G.Coukos[2,11], J. Auwerx[5], M. P. Lutolf[3,14] and O. Naveiras[1,11,12]‡

Supplementary Materials:

- **Supplementary Figure S1:** Transcriptome analysis of NAD pathway genes and influence of NR on the hematopoietic system.
- **Supplementary Figure S2:** NA/NAM-supplementation does not cause hematopoietic progenitor expansion.
- **Supplementary Figure S3:** NR exerts its effect through the NR/Nrk/NMN axis.
- **Supplementary Figure S4:** NR in vitro affects mitochondrial mass and □□m in HSCs.
- **Supplementary Figure S5:** NR improves blood reconstitution and stem cell function of human CD34+ cells.
- **Supplementary Figure S6:** NR induces autophagy, mitophagy, increased OCR and mitochondrial stress.
- **Supplementary Figure S7.** NR induces mitochondrial stress in K562 cells in a dose dependent manner and does not exhaust HSC function in secondary transplantation.
- **Supplementary Table 1:** Oligonucleotide Reference List.

Supplementary Materials:

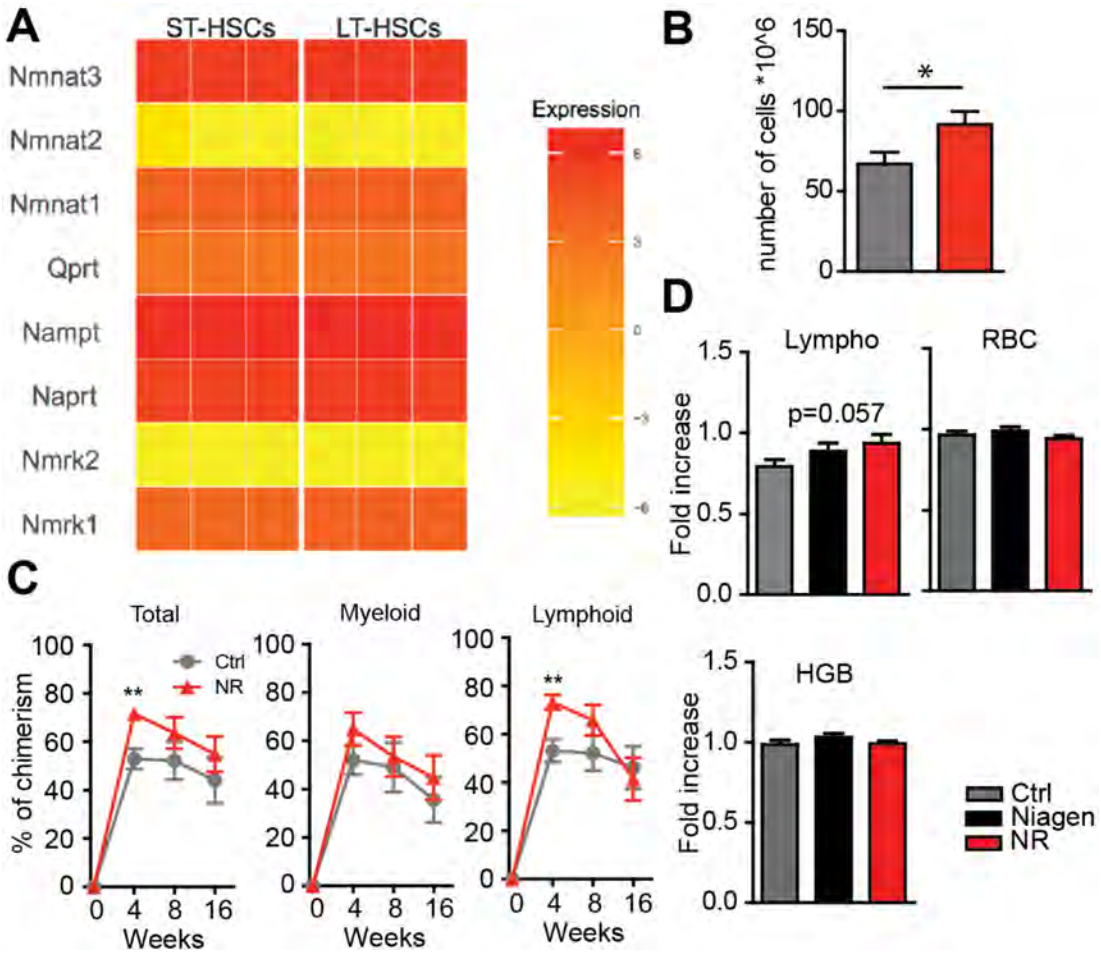

Figure S1. Transcriptome analysis of NAD pathway genes and influence of NR on the hematopoietic system, related to Figure 1. A, Normalized expression for key genes of the NAD salvage pathway in LT-HSCs and ST-HSCs freshly sorted from the bone marrow of 10 week-old C57BL6 females. *n=3.* **B,** BM cellularity of mice fed for 1 week with ctrl or NR diet (legs and hips), *n=5*. **C ,** Blood chimerism of mice transplanted with BM derived from ctrl or NR fed mice was assessed at 4, 8 and 16 weeks, *n=10.* Readings at 16 weeks show no significant difference, indicating that the LT-HSC pool is neither expanded nor exhausted after NR treatment**,** *n=10.* **D,** Analysis of peripheral blood for Lymphocytes, Red blood cells (RBC) and hemoglobin (HGB) in mice fed with ctrl, Niagen or NR diet, *n=5. Student's t test *P<0.05, **P<0.01, ***P<0.001.*

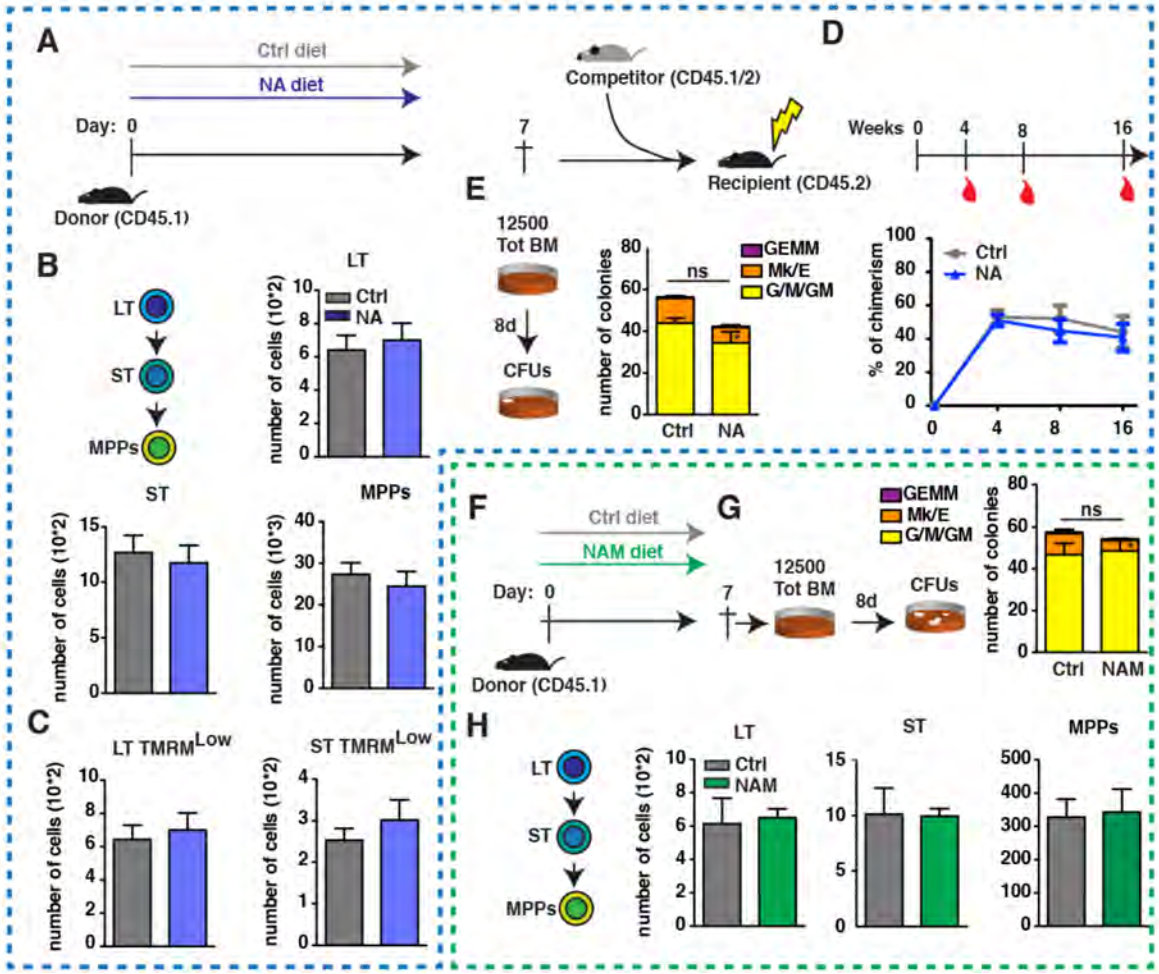

Figure S2. NA/NAM-supplementation does not cause hematopoietic progenitor expansion, related to Figure 1. **A,** Mice were fed 1 week with control or NA diet, mice were sacrificed for BM analysis and primary transplant. **B,** Phenotypic analysis of the different BM hematopoietic stem/progenitor compartments from ctrl or NA fed mice by flow cytometry, *n=5.* **C ,** LT and ST-HSC mitochondrial potential measured by TMRM staining from BM of ctrl or NR diet fed mice, *n=5.* **D,** Blood chimerism of mice transplanted with BM derived from ctrl or NA fed mice was assessed at 4, 8 and 16 weeks, *n=10.* **E,** 12,500 BM cells from ctrl- or NA-fed mice were plated in Methocult for colony forming CFUs analysis 8 days after plating, *n=5.* **F,** Mice were fed 1 week with control or NAM diet, mice were sacrificed for BM analysis and secondary transplants. **G,** 12,500 BM cells from ctrl- or NAM-fed mice were plated in Methocult for colony forming CFUs analysis 8 days after plating, *n=5.* **H,** Phenotypic

analysis of the different BM hematopoietic stem/progenitor compartments from ctrl or NAM fed mice by flow cytometry, *n=5. .. Student's t test *P<0.05, **P<0.01, ***P<0.001.*

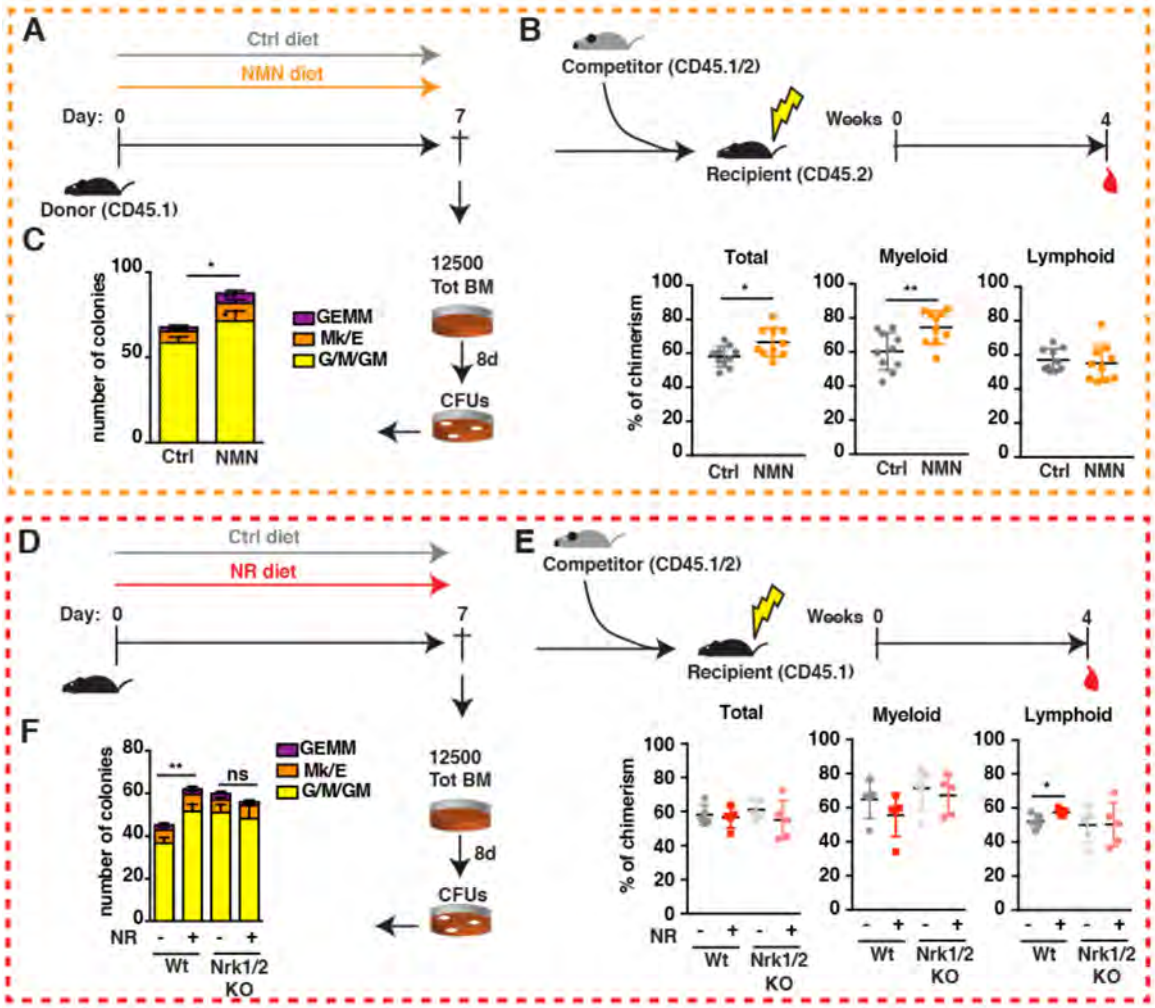

Figure S3. NR exerts its effect through the NR/Nrk/NMN axis, related to Figure 1. **A,** Mice were fed 1 week with control or NMN diet, mice were sacrificed for BM analysis and secondary transplants. **B,** Blood chimerism of mice transplanted with BM derived from ctrl or NMN fed mice was assessed at 4 weeks, *n=10.* **C,** 12,500 BM cells from ctrl- or NMN-fed mice were plated in Methocult for colony forming CFUs analysis 8 days after plating, *n=5.* **. D,** Nrk1-/-;Nrk2-/- double KO mice were fed 1 week with control or NR diet, mice were sacrificed for BM analysis and secondary transplants. **E,** Blood chimerism of mice transplanted with BM derived from wt or Nrk1/2 KO mice fed with ctrl or NR diet was assessed at 4 weeks, *n=10.* **F,** 12,500 BM

cells from wt or Nrk1/2 KO mice fed with ctrl or NR diet were plated in Methocult for colony forming CFUs analysis 8 days after plating, *n=5. Student's t test *P<0.05, **P<0.01, ***P<0.001.*

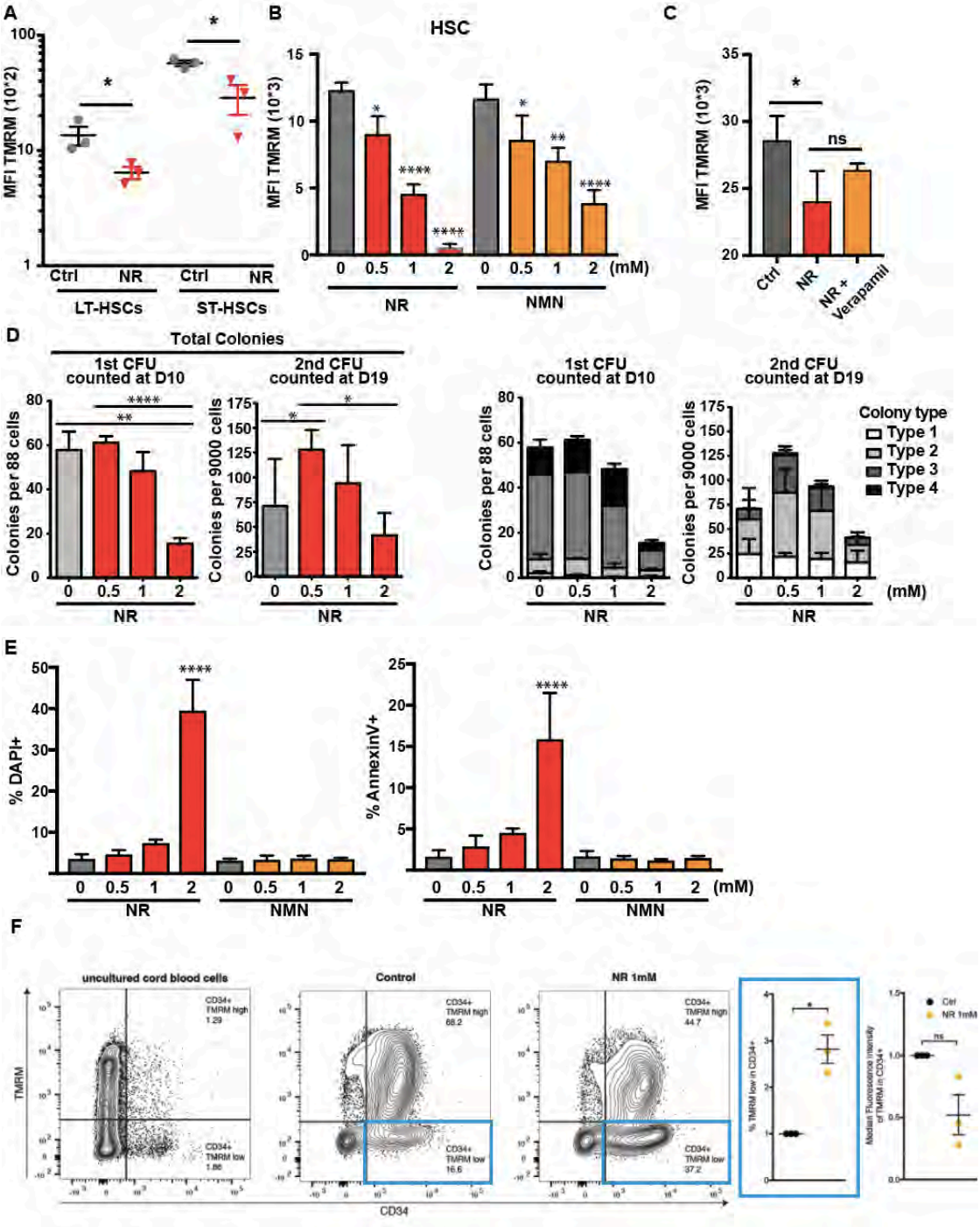

Figure S4. NR *in vitro* affects mitochondrial mass and ΔΨm in HSCs, related to Figures 2-3.

A, LT- and ST-HSCs were FACS sorted and treated in vitro for 48 hours with 0.5 mM NR (A,) or increasing concentrations of NR or NMN (B,), then stained with TMRM and analyzed by FACS. **C,** HSCs were cultured for 48h with NR. The calcium dependent ABC pump inhibitor verapamil was added at 50µM 1 h before TMRM staining and subsequent flow cytometric analysis. There was no significant

difference on the NR-mediated decrease in TMRM signal in presence or absence of verapamil. **D,** HSCs cultured with NR for 48h, were plated in M3434 methylcellulose and their long-term colony-forming capacity was analyzed in secondary CFU assays. CFUs were scored using the StemVision software (StemCell Technologies). Colony type depends on the colony size and cell density, with Type 1 being the smallest and less dense colony. Note that there is no differences in the primary CFU and that the highest NR concentration of 2mM was toxic to murine HSCs, but not to human CD34+ progenitors (Figure 3A). **E,** HSCs cultured with NR or NMN at different concentrations, stained with DAPI and Annexin V, and analyzed by FACS. **F,** Cord blood derived human CD34+ cells were cultured for 2 days in the presence or absence of NR as in Fig. 3A. Shown is the experimental replicate for cord blood in a different laboratory with completely independent donors (upper panel & lower panel). Both the fold change in the $TMRM^{low}$ population (labeled in blue) and the TMRM MFI of total CD34+ were quantified. *n=3.Student's t test *P<0.05, **P<0.01, ***P<0.001*

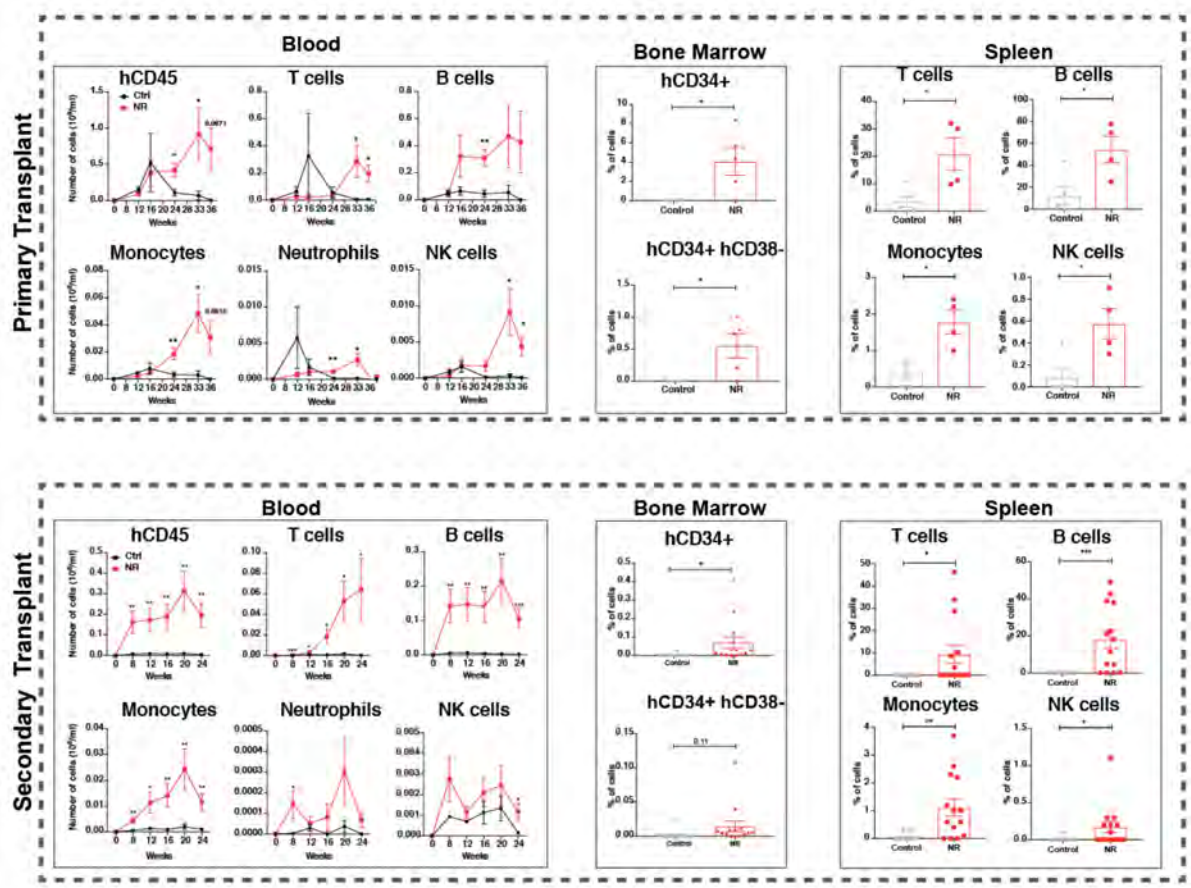

Supplementary Figure S5: NR improves blood reconstitution and stem cell function of human CD34+ cells, related to Figure 3. Fetal derived human CD34+ cells were cultured for 5 days in the presence or absence of NR and transplanted in irradiated NSG mice. Reconstitution of different blood lineages (Blood panels) was followed over time in primary (1^0 Transplant) and secondary (2^0 Transplant) recipient mice. At the endpoint hematopoietic progenitors (CD34+ and CD34+CD38-) and blood lineages were quantified in the bone marrow and spleen of recipients' mice respectively. *n=6 & n=12 . Student's t test *P<0.05, **P<0.01, ***P<0.001.*

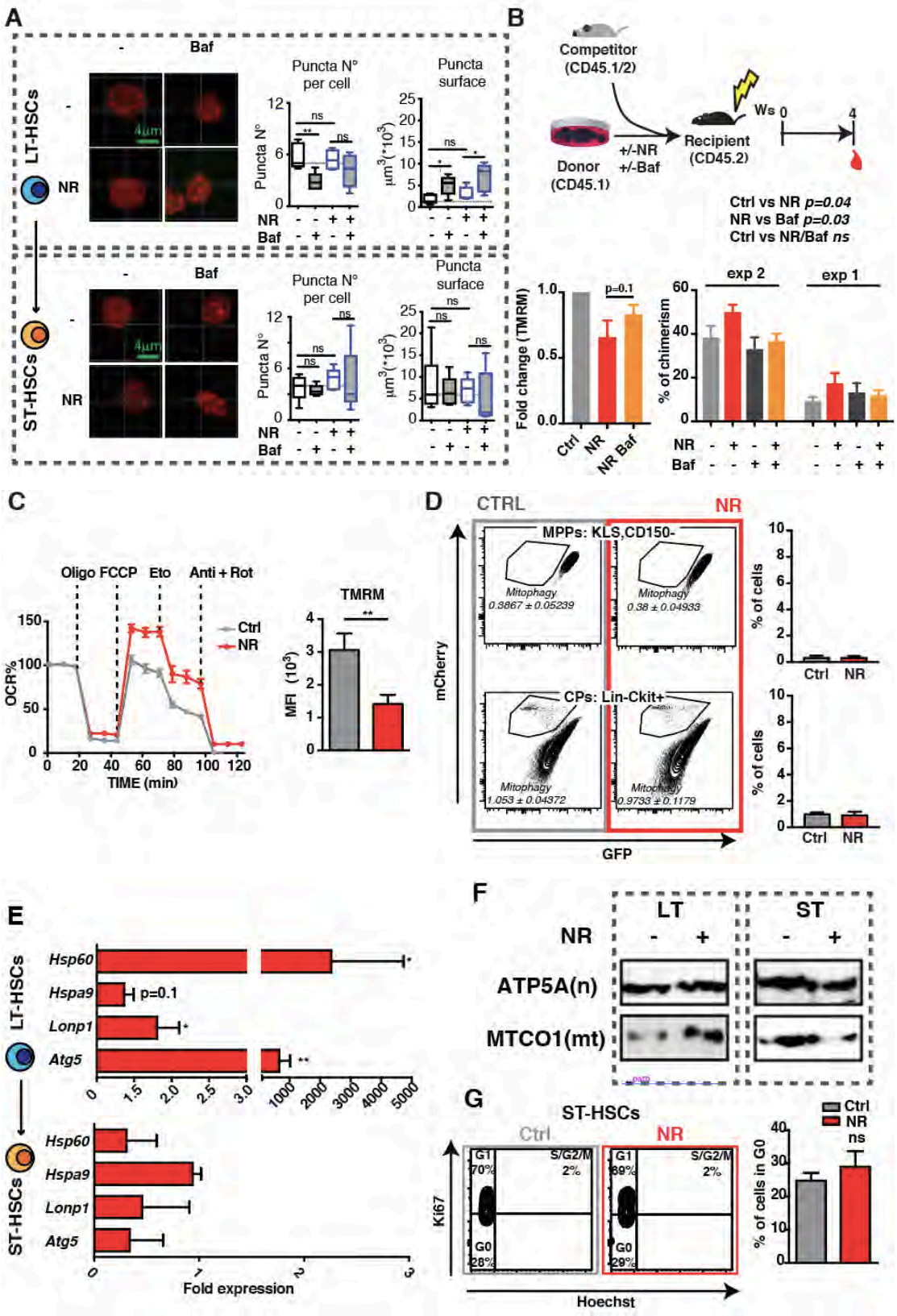

Figure S6. NR induces autophagy, mitophagy, increased OCR and mitochondrial stress; related to Figures 4-5. A, Confocal analysis of HSCs exposed to NR, autophagy blocker Bafilomycin, or both. Cells were stained with Lc3B antibody and number and size of autophagosomes was measured. (Upper panels LT-HSCs; Lower

panel ST-HSCs). **B,** LT-HSCs (CD45.1) were cultured for 2 days in the presence of absence of NR and Bafilomycin (Baf). ΔΨm of HSCs was then analyzed by flow cytometry with TMRM staining in presence or absence of bafilomycin (lower left, n=4). LT-HSCs were cultured for a total of two days and transplanted into lethally irradiated mice (CD45.2) together with total bone marrow competitor cells (CD45.1/2). Engraftment capability was measured by blood analysis in 2 independent experiments (lower right). Statistics are for the combined experiments, which are shown separately because the baseline engraftment was very different for both cohorts. **C,** Splenocyte-derived cells were cultured with NR over 3 days. Oxygen consumption rate (OCR) of splenocyte-derived cells was measured at basal level and in response to oligomycin (Oligo), FCCP, etomoxir (Eto) and antimycin (Anti) in combination with rotenone (Rot) (left panel); and ΔΨm was measured by TMRM staining and analyzed by FACS (right panel). **D,** Mito-QC mice were fed for 1 week with control or NR diet. Percentage of cells undergoing mitophagy was quantified. Downstream hematopoietic progenitors, MPPs (KLS CD150-) and CPs (Lin- cKit+) showed lower mitophagy rates as compared to the most primitive hematopoietic compartments and most importantly, their mitophagy rates were not affected by NR supplementation. **E,** Backgating analysis of Mito-QC cells. In the Mitophagy analysis of LT and ST-HSCs the $mCherry^{high}$ population (left panels) was excluded, as it represented PI^{interm} cells which backgated away from the core HSC population both in the FSC and KLS gates. **F,** Gene expression analysis of ST or LT-HSCs isolated from the BM of NR or control diet fed C57BL6 mice, *n=4*. **G,** Mito-nuclear protein imbalance in HSCs FACS sorted from mice fed control vs. NR diet for 7 day. Western blotting protein analysis of mitochondrial proteins encoded by nuclear subunit (ATP5a) and mitochondrial subunit (MTCO1) of the oxidative phosphorylation complex (see text for interpretation, data derived from the pooled bone marrow of 32 mice). **G,** Cell cycle analysis of ST-HSCs derived from NR or control diet fed mice, *n=5. Student's t test *P<0.05, **P<0.01, ***P<0.001.*

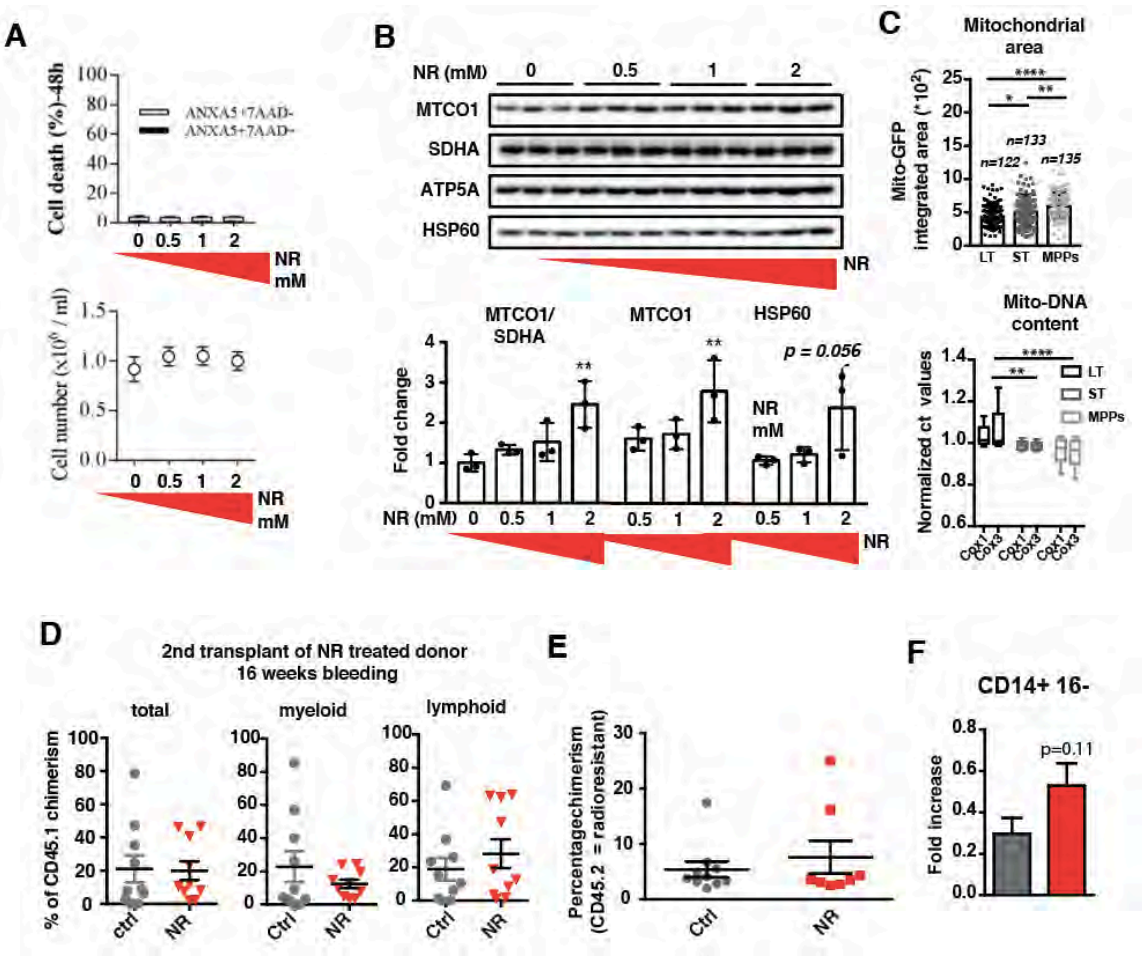

Supplementary Figure S7: NR induces mitochondrial stress in K562 cells in a dose dependent manner and does not exhaust HSC function in secondary transplantation, related to Figure 7.

A, Cell death was assessed by flow cytometry using annexin V (ANXA5) and 7AA D double staining after 48 hours of NR exposure. Absolute cell number was determined by flow cytometry using absolute counting beads. **B,** western blot quantification of NR-driven mito-nuclear protein unbalance (MTCO1/SDHA) and NR-driven induction of UPRmt chaperone HSP60. **C,** Mito-EGFP derived hematopoietic stem and progenitor cells were analyzed for their mitochondrial content. Confocal analysis of single cell integrated EGFP signal was used to quantify mitochondrial area (upper panel). Mitochondrial DNA content was analyzed by QPCR targeting 2 different mitochondrial genes (Cox1 and Cox3). Values are

expressed as normalized ct that inversely correlated to the DNA content (lower panel). **D,** Analysis of radioresistant BM (recipient, CD 45.2+) of transplanted mice with BM derived from ctrl or NR diet fed mice, *n=10.*. **E,** Secondary transplants were performed with total bone marrow from mice having received limiting-dose transplantation while treated with NR or control diet (Figure 7C-D), then analyzed at 16 weeks for persistence of donor CD45.1 stem cell function. **F,** Analysis of CD14+ CD16- monocytes of peripheral blood of humanized mice fed for 7 days with ctrl or NR diet (gated on hCD45), *n=5. Student's t test *P<0.05, **P<0.01, ***P<0.001 and Two-way ANOVA *P<0.05, **P<0.01, ***P<0.001.*

Oligonucleotides
Sirt1-F AGTTCCAGCCGTCTCTGTGT
Sirt1-R CTCCACGAACAGCTTCACAA
Hsp60-F GCTGTAGCTGTTACAATGGGG
Hsp60-R TGACTTTGCAACAGTGACCC
Hspa9-F AATGAGAGCGCTCCTTGCTG
Hspa9-R CTGTTCCCCAGTGCCAGAAC
LonP1-F ATGACCGTCCCGGATGTGT
LonP1-R CCTCCACGATCTTGATAAAGCG
Atg5-F AAGTCT GTCCTTCCGCAGTC
Atg5-R TGAAGAAAGTTATCTGGGTAGCTCA
Arbp-F AGATTCGGGATATGCTGTTGG
Arbp-R AAAGCCTGGAAGAAGGAGGTC

Supplementary Table 1: Oligonucleotide Reference List, related to STAR Methods.

STAR+METHODS

Detailed methods are provided in the online version of this paper and include the following:

REAGENTS

Antibodies

Mouse

cKit (2B8) PE/Cy7
Sca1 (D7) APC
Sca1 (D7) PE
CD150 (TC-15-12F12.2) PE
CD150 (TC-15-12F12.2) PE/Cy5
CD150 (TC-15-12F12.2) BV784
CD48 (HM48-1) PB
CD45 (30-F11)
CD45.2 (104) PB
CD45.1 (A20) FITC
CD34 (RAM) FITC
CD34 (RAM) eF660
Gr1 (RB6-8C5) APC
F4/80 (BM8) APC
CD19 (6D5) PE
CD3 (17A2)
CD16/CD32 (2.4G2)
Biotynilated Lineage Coktail
LC3B
MTCO1
ATP5A
SDHA
HSP 60

Human

hCD56 (NCAM16.2) FITC
hCD16 (3G8) PerCP-Cy5.5
hCD45 (HI30) PE
hCD19 (HIB19) APC
hCD4 (RPA-T4) APC-H7
hCD3 (SK7) eFluor450
hCD14 (M5E2) V500
hCD8b (SIDI8BEE) PE-Cy7
hCD34 (8G12) FITC
hCD38 (HB-7) APC

Biological samples

Cord blood CD34+ cells
Cord blood CD34+ cells
Fetal derived CD34+ cells
Adult derived CD34+ cells

Culture Media and cytokines

Stemline II
StemSpan
RPMI
FCS
Pen/Strep
mouse SCF
mouse Flt3

human SCF
human FLT3L
human TPO
human LDL
MethoCult M3434

Mitochondrial staining & others
TMRM
JC-1
Mitotracker Deep Red
DAPI
PI
CFSE
SAV-PO
SAV-TxRed* not in paper

Reagents
NR triflate
NA
NAM
NMN
ZR RNA MicroPrep
Vilo Script
Power Syber Green mastermix
Protease inhibitor coktails

DC protein assay
Cell Tak
oligomycin
FCCP
rotenone
antimycin
etomoxir
verapamyl
bafilomycin
RBC lysis buffer
human CD34+ selection

Experimental models/ strain
C67Bl/6 J
NSG
MitoQC
Mito-eGFP
NRK1/2 ko

Diet
Chow diet

Treatment of transplanted mice
Amoxicillin (Amoxi-Mepha)
Enrofloxacin (Baytril)
Bactrim (Sufamethoxazole, Trimethoprim)

Paracetamol (Dafalgan®)

Cell lines
K562

RNA-seq
Quick-RNA Microprep Kit
SMART-Seq v4 Ultra Low Input RNA Kit for Sequ
Nextera XT DNA Library Preparation Kit

Softwares
Flowjo Software
FACSDIVA
GraphPad Prism 7
ImageJ
Imaris version 9.2
R

Deposited data
RNA-seq data

SOURCE	IDENTIFIER
Biolegend	105814
Biolegend	108112
Biolegend	108108
Biolegend	115904
Biolegend	115912
Biolegend	115904
Biolegend	103418
Biolegend	103147
Biolegend	109820
Biolegend	110706
eBioscience	11-0341-85
eBioscience	50-0341-82
Biolegend	108412
Biolegend	123116
Biolegend	115507
Biolegend	100206
BD	553141
BD	558451
Cell Signaling	2775
Abcam	ab14705
Abcam	ab14748
Abcam	ab14715
Santa Cruz	sc-1052

BD	345811
BD	560717
BD	555483
BD	555415
BD	560251
Thermo Fisher	48-0036-42
BD	561392
Thermo Fisher	25-5273-42
BD	345801
BD	345807

	n/a
Zürich University Hospita	n/a
"Etablissement de Transfu	n/a
CHUV (Lausanne)	n/a
CHUV (Lausanne)	n/a

Sigma	S0192
StemCell Technologies	9600
Gibco	11875093
Gibco	10270
Gibco	15140
R&D systems	455-MC-050
R&D systems	427-FL-025

Miltenyi	130-096-694
Miltenyi	130-096-477
Peprotech	AF-300-18
StemCell Technologies	2698
StemCell Technologies	3434

Invitrogen	T-668
Cayman Chemical	10009172
Thermo Fisher	M22426
Thermo Fisher	D1306
Sigma	81845
Cayman Chemical	10009853
Thermofisher	S32365
Invitrogen	S872

Novalix	custom synthesis
Sigma	N4126
Sigma	72345
Sigma	N3501
Zymo Research	R1060
Thermo Fisher	11754050
Applied Biosystem	4367659
Thermo Scientific	78430

BIO-RAD	500-0116
BD	CB40240
Sigma	O4876
Sigma	C2920
Sigma	R8875
Sigma	A8674
Sigma	30740
Sigma	V4629
Sigma	B1793
BioLegend	420301
StemCell technologies	18056

Charles River	n/a
Harlan/Coukos lab	n/a
Ping Chih Lab	n/a
Lutolf Lab	n/a
Canto lab	n/a

Envigo	2916

Mepha Pharma AG	n/a
Bayer	n/a
Roche	n/a

UPSA	n/a

Douchosal lab	n/a

Zymo Research	R1050
Takara Bio	634891
Illumina	FC-131-1096

Flowjo	n/a
BD	n/a
GraphPad Sotfware	n/a
www.imagej.net	n/a
Bitplane	n/a
www.r-project.org	n/a

National Center for Biotec	GEO: [...]